

Susitna-Watana Hydroelectric Project Document

ARLIS Uniform Cover Page

Title: Site-specific seismic hazard study plan Section 16.6, Study Completion Report. Attachment 6, Revised intraslab model and PSHA sensitivity results		SuWa 289
Author(s) – Personal: Roland LaForge, Allison Shumway, Lia Lajoie, Jamey Turner		
Author(s) – Corporate: Fugro Consultants, Inc.		
AEA-identified category, if specified: November 2015; Study Completion and 2014/2015 Implementation Reports		
AEA-identified series, if specified: Technical memorandum ; 14-11-TM		
Series (ARLIS-assigned report number): Susitna-Watana Hydroelectric Project document number 289		Existing numbers on document: AEA11-022 16-1411-TM-042514
Published by: [Anchorage : Alaska Energy Authority, 2015]		Date published: April 25, 2014
Published for: MWH and Alaska Energy Authority		Date or date range of report:
Volume and/or Part numbers: Study plan Section 16.6		Final or Draft status, as indicated: v1.0
Document type:		Pagination: iv, 2, 21 pages + [23] pages of plates
Related works(s):		Pages added/changed by ARLIS:
Notes: All other parts of Section 16.6 (the main report and Attachments 1-5 and 7-11) are in separate electronic files due to large file sizes.		

All reports in the Susitna-Watana Hydroelectric Project Document series include an ARLIS-produced cover page and an ARLIS-assigned number for uniformity and citability. All reports are posted online at <http://www.arlis.org/resources/susitna-watana/>



ATTACHMENT 6: REVISED INTRASLAB MODEL AND PSHA
SENSITIVITY RESULTS



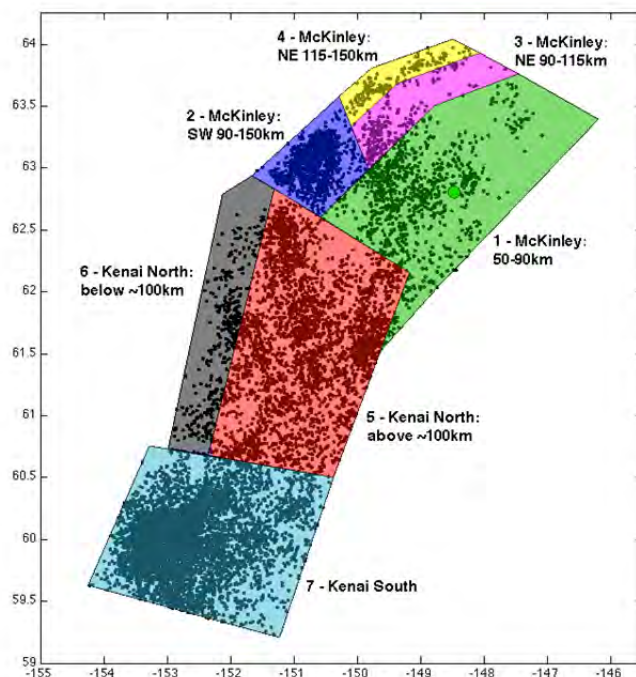
SUSITNA-WATANA HYDRO

Clean, reliable energy for the next 100 years.

Technical Memorandum 14-11-TM v1.0

Revised Intraslab Model and PSHA Sensitivity Results

AEA11-022



Prepared for:
Alaska Energy Authority
813 West Northern Lights Blvd.
Anchorage, AK 99503

Prepared by:
Fugro Consultants, Inc. for MWH
1777 Botelho Drive, Suite 262
Walnut Creek, CA 94596

April 25, 2014

THIS PAGE INTENTIONALLY LEFT BLANK

The following individuals have been directly responsible for the preparation, review and approval of this Report.

Prepared by: Roland LaForge, Allison Shumway, Lia Lajoie, Jamey Turner

Reviewed by: Mike Bruen, Norm Abrahamson, Ron Backner, Dean Ostenaar

Approved by:



Michael Bruen, Geology, Geotechnical, Seismic Lead

Approved by:



Brian Sadden, Project Manager

Disclaimer

This document was prepared for the exclusive use of AEA and MWH as part of the engineering studies for the Susitna-Watana Hydroelectric Project, FERC Project No. 14241, and contains information from MWH which may be confidential or proprietary. Any unauthorized use of the information contained herein is strictly prohibited and MWH shall not be liable for any use outside the intended and approved purpose.

THIS PAGE INTENTIONALLY LEFT BLANK



TABLE OF CONTENTS

EXECUTIVE SUMMARY ES-1

1. INTRODUCTION 1

2. CATALOG DEVELOPMENT AND UPDATE 3

3. SLAB GEOMETRY 5

4. GRID MODELS 8

5. MAXIMUM MAGNITUDES OF INTRASLAB EARTHQUAKES 9

6. PSHA SENSITIVITY CALCULATION RESULTS 15

7. CONCLUSIONS 16

8. REFERENCES 19

List of Tables

Table 2-1. Magnitude Conversions	4
Table 3-1. Slab Plane Parameters.....	7
Table 3-2. Closest Approach Distances of Intraslab Seismic Source	7
Table 4-1. Magnitude – Completeness Periods.....	8
Table 5-1. List of Global Subduction Zones (Modified from Hayes et al., 2012).....	9
Table 5-2. Largest Magnitude (Mmax) Event in Subduction Zone at 100 km Depth or More, or Identified as Non-interface.....	11

List of Figures

Figure 1	AEIC Seismicity, July 1988 – January 2013
Figure 2	Map View of Seismicity in 50-90 km Depth Part of McKinley Block (Plane 1)
Figure 3	View Looking Northeast, Seismicity in Figure 2
Figure 4	3D Depiction of Slab Planes Defined in Northernmost Box of Figure 1 (Planes 1-4)
Figure 5	3D Depiction and Fitted Planes to Seismicity in Middle Box of Figure 1 (Planes 5 and 6)
Figure 6	3D Depiction and Fitted Planes to Seismicity in Southernmost Box of Figure 1 (Plane 7)
Figure 7	Planes Fitted to the Seismicity Shown in Figure 1 Boxes
Figure 8	Cross-Section Diagram Showing Distance Measures in Table 3-2
Figure 9	Map View of Slab Planes
Figure 10	Grid with Correlation Distance = 15 km
Figure 11	Grid with Correlation Distance = 25 km
Figure 12	Grid with Correlation Distance = 35 km
Figure 13	World Oceanic Subduction Zone Regions
Figure 14	Summary Magnitude vs. Depth Plot of all Subduction Zones
Figure 15	Magnitude vs. Depth Plot for Alaska-Aleutian Subduction Zone
Figure 16A	Sensitivity to Mmax, PHA
Figure 16B	Sensitivity to Mmax, 1.0 Second Spectral Acceleration
Figure 17A	Sensitivity to Slab Position, PHA
Figure 17B	Sensitivity to Slab Position, 1.0 Second Spectral Acceleration



SUSITNA-WATANA HYDRO

Clean, reliable energy for the next 100 years.

ALASKA ENERGY AUTHORITY

AEA11-022

16-1411-TM-042514

-
- Figure 18A Sensitivity to Correlation Distance, PHA
Figure 18B Sensitivity to Correlation Distance, 1.0 Second Spectral Acceleration
Figure 19A Sensitivity to Vs30, PHA
Figure 19B Sensitivity to Vs30, 1.0 Second Spectral Acceleration

Explanation of Abbreviations

AEA	Alaska Energy Authority
AEC	Alaska Earthquake Center (formerly known as the Alaska Earthquake Information Center; AEIC)
ASZ	Alaska subduction zone
FCL	Fugro Consultants, Inc.
ISC	International Seismological Centre
km	Kilometer(s)
m	Meter
M	Magnitude
mb	Body wave magnitude
Mw	Moment magnitude
Ms	Surface wave magnitude
Mmax	Maximum magnitude
MWH	MWH Americas, Inc.
PSHA	Probabilistic seismic hazard analysis
TM	Technical memorandum
USGS	U. S. Geological Survey
WSN	Watana Seismic Network

EXECUTIVE SUMMARY

Previous studies (FCL, 2012) indicate that the downgoing slab of the Alaska Subduction Zone (ASZ) comprises the dominant ground shaking hazard to the Watana dam site, compared to other seismic sources in the region. Because the slab geometry in the 2012 model was very simplified (consisting of two constant-depth layers at 60 and 90 km), in this study the geometry was defined by fitting planes to seven sections of the slab in central Alaska, which range in depth from 50 to 150 km. This was accomplished by identifying planes, as revealed in recent seismicity using 3D visualization tools. Strikes, dips, and depth ranges of the seven planes were calculated. These planes were then substituted for the previous two-depth model, and the PSHA was recomputed with the same seismicity rate grid as used in FCL (2012). For the maximum magnitude of M 7.5 used previously, the results were little changed from the 2012 results, and little sensitivity to seismicity grid smoothing parameter, V_{s30} increase from 800 to 1080 m/s, and range of slab positions, was observed.

The thickness of the slab seismicity beneath the site, which is occurring near the top of the slab, appears to be at most about 12 km thick. This is considerably thinner than the thickness of the entire slab, which from tomographic studies in central Alaska appears to be about 50 km. Future large intraslab earthquakes will rupture deeper into the slab than the small-magnitude seismicity data indicates.

A global survey of maximum magnitudes from all significant intraslab environments worldwide shows examples where the magnitude of the largest intraslab earthquake is greater than 7.5. M_{max} in different regions varies between 7.4 to 8.4, with larger M_{max} generally associated with the deeper (400 to 700 km) range. A bimodal pattern appears to be present as the M_{max} decreases from 100 to 400 km in depth but between 400 and 700 km in depth M_{max} increases again.

The question arises as to whether M_{max} on the ASZ downgoing slab, which terminates at about 150 km beneath the site, can be limited due to unique physical conditions that allow M 8.0 – 8.5 events to occur only in the 400 – 600 km depth range. Frohlich (1998, 2006) noted a probable M_{max} dependence on chemical, thermal, and mechanical changes in the slab with increasing depth, but also noted that the historic record (~100 years) is too short to conclude that M_{max} is depth dependent.

There is ambiguity regarding the largest intraslab earthquake in the Alaska-Aleutian arc. There are two possible candidates for largest historic intraslab earthquake: the 1916 Ms 7.4 Fox Islands event, and the 1906 Rat Islands event. There is limited information about the 1916 event, and further study is recommended. The largest appears to be the 1906 event at about 50 km depth, with $M_w = 8.2 - 8.4$. The tectonic origin of this event, however, and whether it could occur in the Watana site vicinity, is unclear. The present evaluation confirms that the M_{max} value of $M_w 7.5$ used in the FCL (2012) analyses must likely be considered a minimum estimate for a M_{max} distribution.



Another important issue to consider is the uncertainty of M_{max} estimates for events in these regions. Many of the largest M_{max} events in each region occurred before 1964, or before the modern worldwide seismograph networks were established. An attempt was made to judge the reliability of the event data using additional published sources, but the reliability of the magnitude estimates for these events is a major source of uncertainty in this study.

PSHA sensitivity studies using the new slab geometry model and maximum magnitudes of 7.8 and 8.1 showed significant sensitivity to this parameter. For a return period of 10,000 years, the $M_{max} = 7.8$ results show a 25% increase in peak horizontal acceleration and 1 second spectral response, and $M_{max} = 8.1$ results show a 50% increase over the $M_{max} = 7.5$ values. However, magnitude scaling of ground motions above $M_w 7.5$ is highly uncertain, and warrants further investigation.

\

1. INTRODUCTION

This report describes a revised intraslab source model for the Alaska Subduction Zone (ASZ) developed from the AEIC (Alaska Earthquake Information Center) earthquake location data that defines the slab geometry, spatial rate variability, and slab extent with relatively high resolution due to the relatively high rates of intraslab activity and the continuing additions of new stations to the AEIC network. The new model updates, and is more refined than that used in the initial, preliminary 2012 Susitna probabilistic seismic hazard analysis (PSHA) study (FCL, 2012). This report also includes PSHA calculations that demonstrate the sensitivity of PSHA results at the Watana dam site from this new intraslab source characterization relative to the previous one. In addition, seismicity catalogues from worldwide subduction zones were reviewed and analyzed to develop additional constraints on the potential maximum magnitude (M_{max}) that might be associated with intraslab seismicity in the ASZ. A range of potential M_{max} values was then evaluated in the PSHA sensitivity analyses.

The intraslab earthquake source of the ASZ lies directly beneath the proposed Watana dam site, and was found in FCL (2012) to be the dominant contributor to the seismic hazard. Therefore, the best possible model is necessary to assure confidence in future engineering analyses of the proposed dam design.

The previous source model essentially adopted that of Wesson et al. (2007), developed for the Alaska component of the U.S. Geological Survey (USGS) National Seismic Hazard Maps. Their intraslab model consists of smoothed, gridded seismicity (Frankel et al., 1996) for two separate depth ranges: 50 – 80 km, and 80 – 120 km. The first set was modeled by a single depth layer at 60 km and the deeper one at 90 km. The “correlation distance,” or standard deviation of the Gaussian smoothing function, was set to 50 km.

For this intraslab characterization and PSHA sensitivity study, the following updates and refinements were made to the USGS model:

1. Updating the USGS earthquake catalog to include events from 2005 through January 2013, and acquisition of AEIC seismicity for the study region.
2. Development of a 3D intraslab model (dipping planes) for the eastern ASZ through examination of AEIC seismicity data from July 1988 through January 2013. Seismicity data from the Watana Seismic Network (WSN), which is a sub-network of the AEIC regional network, was also used, and provided important constraints in establishing the geometry of the downgoing Pacific plate (informally termed the slab). Formal uncertainties of the fit of sub-planes defined from the seismicity cloud along the top of the downgoing slab were computed.



3. Development of 2D earthquake occurrence rate grids using the Frankel et al. (1996) smoothing technique, with three correlation distances. These grids were projected onto the planes developed in step 2.
4. Research into maximum magnitudes of intraslab earthquakes worldwide was conducted. The major subduction zones were delineated (fourteen in total), and earthquakes with magnitude greater than or equal to M 7 were extracted from a global database. In particular earthquakes deeper than 100 km and magnitude greater than 7.5 were investigated, although events of all depths are shown. Wesson et al. (2007) used a Mmax of 7.5, and reviews of FCL (2012) pointed out that Mmax of intraslab events in other tectonic settings have exceeded this value.

PSHA results for the intraslab source were recomputed using the new model. Sensitivities to four model components were investigated: smoothing parameter (correlation distance), Mmax, distance to the slab, and updated Vs30. The calculations used new Vs30 measurements obtained for the seismograph station near the site (FCL, 2014) as an updated estimate of site velocity.

2. CATALOG DEVELOPMENT AND UPDATE

Two seismicity catalogs were used during the course of this study. The first, described below, was used to develop the smoothed seismicity grids used in the PSHA calculations. These events encompass the historic era (1898 through 2012), and include those with magnitude 4 and greater. The second consists of AEIC seismicity located since July 1988 of all magnitudes. This second catalog was used for the purpose of characterizing the geometry of the downgoing slab in central Alaska.

The starting point of the first seismicity catalog for Susitna was to use the already compiled seismicity catalog for Alaska created by the USGS. The USGS 2007 Alaska Hazard Maps catalog (Wesson et al., 2007) was put together from a collection of historic seismicity catalogs and declustered (i.e. aftershocks and other dependent events were removed). However, the catalog only contained events through 2004 and needed to be updated.

The first step was to download the USGS 2007 Alaska Hazard Maps declustered catalog from the USGS website (<http://earthquake.usgs.gov/hazards/products/ak/2007/>). This catalog contained 7,514 events from 1899 through 2004, Mw4+. The second step was to download seismicity data from the EHB catalog (<http://www.isc.ac.uk/ehbulletin/search/catalogue/>) located on the International Seismological Center (ISC) website. The EHB catalog is a subset of the ISC Bulletin, containing data from 1960 to 2008, where the events have been relocated using the Engdahl (2006) algorithm to improve locations and focal depths. This catalog contained 2,487 events from 1960 through 2008, M3+. The third step was to incorporate the AEIC catalog (http://www.aeic.alaska.edu/html_docs/db2catalog.html). This catalog contained 11,764 events from 2009 through January 31, 2013, with magnitudes greater than M 1.9.

The fourth step was to sort each catalog so that only events within the Susitna project site were chosen (58° to 65° N, -158° to -144° W). Each catalog was also sorted by magnitude (M4+) and depth (31 km+). All the events in the Wesson et al. (2007) declustered catalog had already been converted to moment magnitude (Mw). The EHB catalog and AEIC catalog events that were not already in Mw were converted to Mw in step five using the same formulas used by Wesson et al. (2007) to convert to Mw (Table 2-1).

Table 2-1. Magnitude Conversions

For $M_s < 5.8$, $M_w = 0.75*(M_s+1.93)$
For $M_s > 7.8$, $M_w = 1.50*(M_s-2.60)$
For $5.8 \leq M_s \leq 7.8$, $M_w = M_s$
For $m_b < 5.5$, $m_b = M_w$
For $M_L > 6.5$, $M_w = 1.67*(M_L-2.60)$
For $M_L \leq 6.5$, $M_w = M_L$

The sixth step was to decluster the EHB catalog and AEIC catalog using the Gardner and Knopoff (1974) method. The USGS Alaska catalog had already been declustered; therefore, declustering was not necessary.

The three catalogs were then combined in the seventh and final step, creating a final Susitna seismicity catalog for the project site. The final Susitna catalog is a compilation of the Wesson et al. (2007) declustered catalog, the EHB catalog, and the AEIC catalog. There are 1,264 events from 1911 through January 2013, with M_w greater than or equal to 4.

This catalog, termed the recurrence catalog, was used in the construction of the smoothed seismicity grids.

The second catalog was used for the purpose of developing a geometric model of the slab beneath the site and central Alaska. Post July, 1988 hypocentral locations from the AEIC network were judged to be adequate for this purpose (N. Ruppert, pers. comm., 2013). Earthquakes of all magnitudes in the study region from July 1988 through January 2013 were obtained from the AEIC website. This catalog, which contains 21,916 earthquakes, is termed the AEIC catalog in future discussions. No other modifications, such as declustering, were performed on this catalogue.

3. SLAB GEOMETRY

It has been recognized that the ASZ is segmented in central Alaska, and may be broken into independent fragments (e.g., Ratchkovski and Hansen, 2002). In addition, it has been recognized that the ASZ's eastern termination lies within 100 km northeast of the Watana site (Fuis et al., 2008). The precise location and geometric character of the slab edge are not well determined.

Figure 1 shows seismicity from the AEIC catalog with depth > 30 km, with depths segregated into 10 or 20 km ranges. The 30 km depth is the approximate location where the slab begins to descend into the upper mantle (Ratchkovski and Hansen, 2002). The general northwest-dipping structure of the slab is evident in this figure. Also evident is its segmented nature, described from a similar dataset by Ruppert and Hansen (2002), who defined three major sections of the slab, which they termed the McKinley, Kenai, and Kodiak Blocks. The northernmost section, the McKinley Block, defines the northeast edge of the slab, which appears to terminate at about latitude 64N. The Kenai Block extends from the McKinley Block to about 59.5N, and shows a strike change of about 30 degrees to the south. South of 59.5N the Kodiak Block indicates another strike change of about 30 degrees, but to the west. Due to its distance from the site (> 400 km) the Kodiak Block is not considered in this study.

Inspection of the data in Figure 1 with 3-dimensional visualization software led to the delineation of the black boxes shown on Figure 1 as candidates for the identification of dipping planes having a common strike and dip. The northernmost box, coincident with the McKinley Block, clearly shows a moderately dipping upper section between 50 and 90 km, and a generally more steeply dipping section between 90 and 150 km. The middle and southern boxes comprise the Kenai Block. A division was made at about 60.5N based on a small change in the strike of the depth contours, and a denser pattern of seismicity in the southernmost block. A notable pattern seen in Figure 1 is that regions of dense seismicity are associated with the block boundaries, especially at depths > 100 km. An evaluation of whether these block boundaries represent tears, as opposed to warps in the slab is beyond the scope of this study.

Seismicity in each of these boxes was segregated, and examined in computer software that permitted interactive variation of viewing angle, selection of data subsets, and computation of least-squares best-fit to a plane. Figure 2 shows a map view of seismicity in the 50-90 km depth part of the McKinley Block, which includes the Watana dam site. Figure 3 shows the view from within the earth looking northeast, with the fitted plane shown. The McKinley Block box showed varying contortions and/or slab fragments in the lower portion (90 – 150 km depth) that proved difficult to fit a single plane to; therefore subsets of the lower depth seismicity were defined. Figure 4 shows the resulting plane configuration of the McKinley block box.

Figure 5 shows the two planes defined by the middle box in Figure 1, and Figure 6 shows that the southernmost block in Figure 1 was fit by a single plane.

Figure 7 shows a view looking to the northeast, of all planes fitted by this procedure.

The next step was to adjust the fitted planes in map view so that they formed a continuum to provide consistency with the slab interface part of the model, and extend the deeper part of the McKinley Block slabs to the north, where seismicity indicates the slab must exist (Figure 1). The resulting slab configuration in map view is shown in Figure 9, with slab planes labeled numerically and referenced in Table 3-1. The slab plane depth ranges, strikes and dips, and thickness of seismicity are shown in Table 3-1.

It is important to note that the seismicity shown here occurs within and near the top of, the downgoing slab however, the thickness of the slab is significantly greater. Tomography studies estimate the slab thickness in continental Alaska to be 45-55 km (Zhao et al., 1995). Using intraslab earthquakes that have occurred in the Juan de Fuca plate beneath Puget Sound as an analog (Ichinose et al., 2006), larger magnitude events occurring within the slab (in the M 6-7 range) will rupture deeper into the slab than this data set indicates.

For each plane, a linear least-squares regression through the seismicity provides a best-fit plane to the dataset, representing the average location of seismicity in the slab segment. Slab seismicity thicknesses were calculated using one or two standard deviations of the normal distances from each earthquake to the best-fit plane, thus approximating the seismically active part of the slab as shown by these small-magnitude events, as the volume encompassing 68% and 95% of the seismicity, respectively. For the region encompassing the proposed Watana dam location (Plane 1), a second calculation of the slab geometry and slab seismicity thickness using the WSN since its establishment in November 2012 provides a more accurate representation of the slab. To maintain geometric consistency, the plane parameters from AEIC data were adopted for the PSHA.

Table 3-1. Slab Plane Parameters

Plane Number	Location	Depth Range (km)	Strike	Dip	Slab Seismicity Thickness: 1 σ (km)	Slab Seismicity Thickness: 2 σ (km)
1	McKinley Block (AEIC)	35-90	58	25	4.5	9.0
1	McKinley Block (WSN)	35-90	63	21	6.2	12.3
2	McKinley Block	90-150	52	50	5.5	10.9
3	McKinley Block	90-115	50	32	3.6	7.2
4	McKinley Block	115-150	50	64	4.0	7.9
5	Kenai Block North	40-100	17	27	7.8	15.6
6	Kenai Block North	100-150	11	52	9.2	18.4
7	Kenai Block South	50-200	26	46	9.2	18.3

For deterministic analyses, Table 3-2 shows revised minimum distances and depths to the intraslab source. As shown in Figure 8, distance measures needed for ground motion calculation are nearest distance to the plane, and hypocentral depth (vertical distance to plane). The +1 and +2 sigma values are also shown in the table, as this represents uncertainty in these parameters.

Because the GMPEs used FCL (2012) use hypocentral distance as opposed to closest distance to rupture, these distances will give the most conservative assessment of deterministic ground motions. In order to correctly calculate such amplitudes, potential hypocenters need to be uniformly distributed over the potential rupture surface in the slab, with an area appropriate for the magnitude considered. The average ground motion from that set of hypocenters computed is then the appropriate deterministic value.

FCL (2012) used a nearest distance to the slab of 50 km for their deterministic ground motions calculations. The distances calculated here are 4, 7, and 1 km farther for Best Fit, +1 sigma, and +2 sigmas, respectively.

Table 3-2. Closest Approach Distances of Intraslab Seismic Source

Plane	Nearest Distance to Plane (km)	Vertical Distance to Plane(km)
Best Fit	57.1	62.9
+1 Sigma	54.0	59.5
+2 Sigma	50.9	56.1

4. GRID MODELS

The recurrence seismicity catalog described in Section 2.0 was used as input to the grid development procedure. The catalog was filtered by the same magnitude-completeness periods used in FCL (2012), shown in Table 4-1. Smoothed seismicity occurrence rate grids were generated using the Frankel et al. (1996) technique, for correlation distances of 15, 25, and 35 km. Although Wesson et al. (2007) used a correlation distance of 50 km, the similarity of seismicity patterns seen in Figure 1 and Figure 9 indicates that lesser levels of smoothing are appropriate.

Table 4-1. Magnitude – Completeness Periods

Magnitude Range	Completeness Period
4.0 - 5.0	1/1964 – 1/2013
5.0 - 6.0	1/1964 – 1/2013
6.0 - 7.0	1/1932 – 1/2013
7.0 - 8.0	1/1898 – 1/2013

A maximum-likelihood recurrence calculation (Weichert, 1980) was made for the recurrence catalog described in Section 2.0, for events in the area of Figure 1 with depths of 40 km and greater. The computed b-value of 0.903 is intermediate between the Wesson et al. (2007) values for the entire ASZ of 0.858 for seismicity between 50 and 80 km depth, and 1.007 for events between 80 and 120 km depth.

Occurrence rate grids were created for the area shown in Figure 1, and then sorted so that only grid points within the final intraslab source zone boundaries in Figure 9 were used in the PSHA. The grid points were then projected onto three planes: the mean or best fit, and the other two defined by the +/- 2-sigma distances from the best fit plane. Thus nine total grids (three correlation distances times three slab positions) were created for the PSHA sensitivity analyses. As in Frankel et al. (1996), rates are in terms of 10^a , where a is defined in the incremental form of the Gutenberg-Richter recurrence formula

$$\text{Log}(N) = a - b (M)$$

where N is the number of events between magnitude $M - dm$ and $M + dm$, and dm is 0.05. The 3 occurrence rate grids, along with the seismicity used to generate them, are shown in map view in Figures 10, 11, and 12. Occurrence rate grids projected onto the dipping planes look identical in map view for each of the fit positions (mean, +1 sigma, and +2 sigma), but have differing site to source distance measures for earthquake ground motion attenuation.

5. MAXIMUM MAGNITUDES OF INTRASLAB EARTHQUAKES

It has been recognized that the Mmax of Mw 7.5 for intraslab events used in Wesson et al. (2007) and adopted in the earlier preliminary PSHA study of FCL (2012) appears to have been underestimated, given the known occurrence of larger intraslab earthquake events recorded worldwide (e.g., the M 8.3 10/4/1994 Kurile event at 50 km depth (suggested to be an intraslab event by Tanioka et al. (1995)), the M 8.1 6/16/1910 event at 100 km depth in the Vanuatu Islands, and the M 8.1 11/24/1914 event at 371 km depth near the Bonin Islands) Therefore, a study of the largest magnitudes occurring in subduction zones worldwide was undertaken, with a focus on non-interface (for example, the 1964 Mw 9.2 Alaska which occurred on the plate interface) earthquakes.

Hayes et al. (2012) identified regions around the world where subduction zones are located and created 3D models of these global subduction zone geometries. The Hayes et al. (2012) subduction zones were used for this study, as well as one additional region where subduction is occurring in the eastern Caribbean Sea (Lesser Antilles subduction zone) (see Table 5-1 below). A map of these zones is shown in Figure 13.

Table 5-1. List of Global Subduction Zones (Modified from Hayes et al., 2012)

Region	Abbreviation
Alaska-Aleutians	Alu
Caribbean-Lesser Antilles	Car
Central America	Mex
Cascadia	Cas
Izu-Bonin	Izu
Kermadec-Tonga	Ker
Kamchatka/Kuriles/Japan	Kur
Philippines	Phil
Ryukyu	Ryu
Santa Cruz Islands/Vanuatu/Loyalty Islands	Van
Scotia	Sco
Solomon Islands	Sol
South America	Sam
Sumatra-Java	Sum

The first step in the study was to determine the boundaries of the subduction zones listed in Table 5-1 above. This was done by simply drawing rectangular boxes around the subduction zone geometries identified by Hayes et al. (2012). For the Caribbean-Lesser Antilles region, a rectangular box was drawn around the Lesser Antilles subduction zone.

The second step was to download seismicity data for each of the subduction zones using the boundaries identified in step one. Seismicity data was downloaded from the International Seismological Center (ISC). Seismicity data was first downloaded from the ISC Bulletin (<http://www.isc.ac.uk/iscbulletin/search/catalogue/>). The ISC Bulletin contains data from 1904 to present day and is “regarded as the definitive record of the Earth’s seismicity” (ISC, <http://www.isc.ac.uk/iscbulletin/>). Seismicity data was also downloaded from the EHB Bulletin (<http://www.isc.ac.uk/ehbulletin/search/catalogue/>), also located on the ISC website. The EHB catalog is a subset of the ISC Bulletin, containing data from 1960 to 2008, where the events have been relocated using the Engdahl (1996) algorithm to improve locations. Only M7 and greater events were downloaded, as the purpose of the study was to identify the maximum magnitudes occurring in the intraslab portion of the subduction zones.

The third step was to combine the ISC Bulletin and EHB catalog seismicity data for each subduction zone area. If an event was listed in both the ISC Bulletin and the EHB catalog, the EHB catalog was considered the authoritative listing, as this catalog data contains more accurate hypocenters. Once a seismicity catalog was complete for a rectangular subduction zone region, the catalog was sorted using the subduction zone geometry coordinates provided by Hayes et al. (2012) and events falling outside of the zone boundaries were removed.

The fourth step in the study was to make plots of the seismicity catalogs at each subduction zone showing Magnitude vs. Depth (km). This approach was modeled after Frohlich (1998). This gave a visualization of the magnitude ranges that are occurring at each of the subduction zones, as well as the depths of the events.

We considered intraslab events to be those occurring at 100 to 400 km, but we also took note of events occurring in the deep part of the slab (> 400 km). The 100 km upper limit was selected to exclude interface earthquakes. However, well-located slab events are known to occur at depths shallower than 100 km (e.g., Ichinose et al., 1996), and the depth extent of interface earthquakes worldwide appears to vary between 20 – 60 km, depending on the subduction zone (Tichelaar and Ruff, 1993). Depth errors for earthquakes in the 50 – 100 km range in this dataset are likely to be on the order of tens of kilometers, especially for pre-1960 earthquakes that have not been the subject of special studies. Therefore it is generally not possible to distinguish slab events from interface events in the 50 – 100 km depth range given the limitation of the dataset and the scope of this report.

The fifth step of the study included determination of the largest magnitude events occurring at 100 km or more for each subduction zone region. A summary of the Mmax at each subduction zone is shown in Table 5-2 below. Figure 14 is a summary Magnitude vs. Depth plot of each subduction zone region.

Table 5-2. Largest Magnitude (Mmax) Event in Subduction Zone at 100 km Depth or More, or Identified as Non-interface

Region	Mmax (Depth 100 to 400 km)	Mmax (Depth > 400 km)
Alaska-Aleutians	7.4 or 8.35 ¹	N/A
Caribbean-Lesser Antilles	7.5	N/A
Central America	7.4	N/A
Cascadia	N/A ²	N/A
Izu-Bonin	8.1	7.5
Kermadec-Tonga	7.9	7.8
Kamchatka/Kuriles/Japan	8.3 ³	8.3
Philippines	N/A ²	N/A
Ryukyu	7.9	N/A
Santa Cruz Islands/Vanuatu/Loyalty Islands	8.1	N/A
Scotia	7.6	N/A
Solomon Islands	7.5	7.3
South America	7.8	8.2
Sumatra-Java	7.4	7.5

1. 8/17/1906 Mw 8.35 event occurred at ~50 km depth, but was identified by Okal (2005) as a non-interface event. Other evidence suggests it may not have been a slab event either (see text). The largest clearly intraslab Alaska-Aleutian event is the Ms 7.4 earthquake of 4/18/1916, at a depth of 170 km.
2. All events occurring in Cascadia and Philippines are less than 100 km in depth, but intraslab events are found in these subduction zones at shallower depths (e.g. the 4/13/1949 M 7.1 (60 km depth), 4/29/1965 M 6.7 (60 km depth), and 2/28/2001 M 6.8 (56 km depth) events in the Cascadia subduction zone).
3. 10/4/1994 M 8.3 event occurred at 50 km depth, but was identified by Tanioka et al. (1995) as an intraslab event.

The last step in the study was to attempt to judge the reliability of the largest magnitude values in each seismicity catalog. For the Izu-Bonin, Kermadec-Tonga, Ryukyu, Santa Cruz Islands/Vanuatu/Loyalty Islands, Scotia, South America, and Alaska-Aleutians seismicity catalogs, the Mmax events in the intraslab all occurred before 1964, or before the modern worldwide seismograph networks were established. The information for how these events were recorded, and the quality of the locations, depths, and magnitude estimates, is not readily available for these regions. The main sources that were used to verify the pre-1964 event information in the subduction zone catalogs (that originated from the

ISC and EHB catalogs) were from Abe (1981) and Huang et al. (1997, 1998). Abe (1981) contains a catalog of large shallow, intermediate, and deep earthquakes from 1904 through 1980. Huang et al. (1997) produced centroid moment tensor solutions for deep earthquakes from 1907 to 1961 and Huang et al. (1998) produced centroid moment tensor solutions for deep earthquakes from 1962-1976. Each pre-1964 large magnitude event in each of the subduction zone catalogs was searched for in these. When a discrepancy was found, results from Abe (1981) and Huang et al. (1997, 1998) were considered to be authoritative and the locations, depths, and magnitudes in the subduction zone catalog were updated.

Figure 14 shows the pattern also seen by Frohlich (1998, 2006); that M_{max} of earthquakes from 100 – 400 km depth appears to decrease with depth, but between 400 and 600 km appear uniformly high, with two between 8.0 and 8.5. The question arises as to whether M_{max} on the ASZ downgoing slab, which terminates at about 150 km beneath the site, can be limited due to unique physical conditions that allow M 8.0 – 8.5 events to occur in the 400 – 600 km depth range, but not shallower.

Frohlich (2006; section 4.4.5, “Is maximum size depth dependent?”) addresses this question. While stating that it is plausible that M_{max} is depth dependent due to chemical, thermal, and mechanical changes as the slab descends into the mantle, the short (~100 year) recording period of the instrumental era of seismology precludes such a conclusion, and that “...there is no compelling evidence that the maximum size of deep earthquakes depends on focal depth.”

A search was also done for every magnitude > 7.5 event in each catalog to see if the event was listed on the USGS website of Historic World Earthquakes (<http://earthquake.usgs.gov/earthquakes/world/historical.php/>). A literature search was also done for each large magnitude event in each catalog to see if any special studies had been performed that could verify the event information. Most of the pre-1964 events were not listed on the USGS website of Historic World Earthquakes and no special studies were found. For most pre-1964 events, Abe (1981) and Huang et al. (1997, 1998) were the only sources to obtain refined location, depth, and magnitude. Because of this, the locations, magnitudes and depths of the pre-1964 events should be considered with some caution when considering this data as evidence for M_{max} .

The results show a number of intraslab earthquakes above M 7.5 in the subduction zone catalogs. In the Izu-Bonin catalog, there is an M 8.1 event on 11/24/1914 at 371 km depth. In the Kermadec-Tonga catalog, there is an M 7.9 event on 1/1/1919 at 180 km depth. In the Kamchatka/Kuriles/Japan catalog, there is an 10/4/1994 event at 50 km depth. Tanioka et al. (1995) state the magnitude of this event as M_w 8.3 and estimated the focal depth at 50 km. While this event appears to have ruptured at a more shallow depth than most intraslab earthquakes, Tanioka et al. (1995) conclude this event to be an intraslab event, not an interface event, due to its mechanism. They suggest that it was a result of the tearing of the slab, as opposed to the commonly assumed mechanisms of slab pull due to gravity and/or

push from the spreading ridge that created the plate. In the Ryukyu catalog, there is an M 7.9 event on 6/15/1911 at 160 km depth. In the Santa Cruz Islands/Vanuatu/Loyalty Islands catalog, there is an M 8.1 event on 6/16/1910 at 100 km depth. In the Scotia catalog, there is an M 7.6 event on 9/8/1961 at 103 km. In the South America catalog, there is an M 7.8 event on 11/29/1957 at 162 km. Note that all these events, except the 10/4/1994 Mw 8.3 event in the Kamchatka/Kuriles/Japan catalog, are pre-1964 events.

Figure 15 show magnitude vs. depth for the ASZ. The symbols in red indicate there are two possible candidates for largest historic intraslab earthquake: the 4/18/1916 Ms 7.4 Fox Islands event, and the 8/17/1906 Rat Islands event. This ambiguity is reflected in Table 5-2.

The August 17, 1906 earthquake was analyzed by Okal (2005), who used a set of original seismograms to invert for location, depth, and moment tensor (focal mechanism). His conclusions were that the spectral ratio of Love to Rayleigh waves precluded this from being a typical interface thrust earthquake, and thus had to be a non-interface event. The best fit focal mechanism shows normal faulting on north-south planes, perpendicular to the arc, clearly not thrust as one would expect for an interface event. The depth estimate is 40-60 km, with a best fit at 50 km. A seismic moment of 3.8×10^{28} dyne-cm was computed. The formula of Hanks and Kanamori (1979), $M_w = 2/3 \times \log(\text{seismic moment}) - 10.7$ yields a moment magnitude (M_w) of 8.35. To test the robustness of the seismic moment estimate Okal (2005) varied the seismograph station gains +/- 25%, and found the seismic moment varied between -13% and +12%. From the moment to M_w equation above this implies a range of M_w 8.3 to 8.4. They state the solution was not sensitive to the amount of damping introduced in the inversion process.

Other magnitude estimates for this event are listed in Geller and Kanamori (1977). In addition to Ms 8.0 in Gutenberg and Richter (1954), they list 8.3 from Duda (1965), 8.3 from Richter (1958), and Ms 8.2 and mb 7.8 from "Gutenberg-Richter notes". It is thus likely that the Ms 7.8 from ISC is actually mb. Geller and Kanamori (1977) point out that the magnitude, listed as PAS in the ISC catalog, is actually a combination of mb and Ms magnitudes.

The M_w scale is used in modern hazard analysis, since the ground motion prediction equations use it in their regressions. Kanamori (1977) showed that for subduction zone interface earthquakes Ms is equivalent to M_w up to about Ms 8.5. The agreement between the Okal (2005) magnitude estimate and earlier ones listed in Geller and Kanamori (1977) suggest that this earthquake had a magnitude in the M_w 8.2 – 8.4 range.

The tectonic origin of the August 17, 1906 earthquake is unclear. Okal (2005) suggests that it may represent a slab-tearing event, similar to a 1994 Mw 8.3 Kurile event (Tanioka et al, 1995), due to its proximity to Bower's Ridge, a fossil island arc north of the Aleutian arc. Another possibility is that it represents normal faulting in the overriding plate above the slab due to oblique subduction, similar to a

Ms ~7.5 event that occurred in the Lesser Antilles, Caribbean arc, at a similar depth in 1974 (McCann et al., 1982). The 1906 Aleutian event had a normal mechanism with fault planes perpendicular to the arc, and tension axis parallel to the strike of the arc. These observations are identical to those seen for the 1974 Caribbean event. Similar normal faulting in the overriding plate has been seen in the Aleutian arc about 100 km east of the Okal (2005) location (LaForge and Engdahl, 1979). The 1906 event therefore may not have occurred in the slab at all, but in the overriding North American plate, with oblique subduction as the cause.

The results of the Okal (2005) analysis have implications for the Ms 7.4 1916 Fox Islands event, seen at a depth of 170 km in Figure 15. If its Ms of 7.4 is based on surface wave amplitudes, its moment magnitude is likely underestimated. This is because surface waves, which use the earth's crust as a waveguide, are not well generated by an earthquake occurring so deep in the mantle. The crust in this location is 40 km at most (Janiszewski et al., 2013). The fact that the 1916 Fox Islands earthquake doesn't appear in historic seismicity catalogs (e.g., Geller and Kanamori, 1977; Richter, 1958) suggests that it may have been smaller than the 8/17/1906 earthquake.

If sufficient seismograms exist, a study of the 1916 event similar to the Okal (2005) analysis of the Rat Islands event would be important in refining its magnitude, location, and depth, as well as computing a focal mechanism. Investigations into whether the 1906 earthquake was a slab event or not, and whether oblique subduction played a dominant role in its occurrence, are important to judging the possibility of such an event occurring beneath the Watana site, where oblique subduction is minimal.

A rigorous analysis of what Mmax distributions for intraslab events should be used in future PSHAs for the Watana site is beyond the scope of this study. However, this review of large magnitude slab events associated with the Alaska and other subduction zones indicates that an upper bound value for future Mmax distributions used in the final PSHA analysis is likely to lie between 8.0 and 8.5. For this sensitivity analysis Mmax values of 7.5, 7.8, and 8.1 are used, although Figures 14 and 15 suggest magnitudes greater than 8.1 are possible.

6. PSHA SENSITIVITY CALCULATION RESULTS

PSHA hazard sensitivity for the intraslab source was computed using the model described here. The ground motion prediction equations (GMPEs) and their weighting were the same as in FCL (2012). A total of 27 results were computed: all combinations of three correlation distances, three slab positions, and three Mmaxes. Hazard curves for peak horizontal acceleration (PHA) and 1.0 second spectral acceleration response (5% damping) were computed. These are portrayed for the purpose of comparing the three sets of input parameters to each other, in addition to determining the overall difference in hazard from the FCL (2012) results. No weighting of the alternative values is included in this analysis.

In addition, new IMASW site response studies were conducted in the summer of 2013 (FCL, 2014), which resulted in a higher Vs30 estimate for the site (1080 m/s) than the 800 m/s value used in FCL (2012). The PSHA hazard sensitivity to this higher Vs30 value is also shown.

Sensitivity of the new intraslab source model to the three Mmax estimates are shown in Figures 16a and 16b. A Vs30 of 800 m/s, as in FCL (2012), was used in this and the following comparisons. The correlation distance and slab position were set to 25 km, the mean slab position, and an Mmax of 7.5. The first observation is that hazard curves are close to the 2012 results, indicating that the Wesson et al. (2007) geometric slab model gives similar results for this site and these response periods, for an Mmax of 7.5. The second observation is that the results are very sensitive to choice of Mmax. For PHA, at a 1/10,000 annual frequency of exceedance (AFE) the ground motion increases from about 0.8 to 1.2 g as Mmax increases from M7.5 to M8.1, an increase of 50% in ground motion. For 1.0 second response the increase is comparable.

Sensitivity of the PSHA hazard results to the three slab positions for the new model is shown in Figures 17a and 17b. Mmax was set to 7.5, and correlation distance to 25 km. These figures show that there is essentially no sensitivity to this parameter in the computed PSHA hazard.

Sensitivity of the PSHA hazard results to the three correlation distances for the new model is shown in Figures 18a and 18b. Mmax was set to 7.5, and slab depth to the mean position. These figures show that there is negligible sensitivity to this parameter.

Sensitivity of the PSHA hazard results to the use of Vs30 = 800 m/s vs. of Vs30 = 1080 m/s (FCL, 2014) as the site characterization inputs is shown in Figure 19a and 19b. For this analysis and Mmax of 7.5, correlation distance of 25 km, and the mean slab depths were used. These figures show very little sensitivity to the two Vs30 values.

7. CONCLUSIONS

This study resulted in a more physically realistic geometric model of the downgoing Pacific plate in the vicinity of the site for use in PSHA and ground motion analyses, based on planes fitted to well-located seismicity. These analyses confirm earlier suggestions (e.g. Ratchkovski and Hansen, 2002) that the subducting plate beneath southern and central Alaska consists of several segments or sections with distinctly differing dips and orientations. For each of the geometrically distinct slab sections defined by seismicity, best fit planes with 1σ and 2σ bounding limits were defined to characterize the upper slab surface. For the intraslab section most proximal to the Watana site, 1σ and 2σ limits of slab seismicity thickness are 9.0 and 12.3 km, respectively, with dip calculations of 21 and 25 degrees (Table 3-1). The $+2\sigma$ uncertainty for the best fit plane has a closest approach to the Watana site of 51 km, and depth beneath the site is 59 km. The best fit plane has a closest approach of 57 km and depth beneath the site of 63 km.

Slab thickness in central Alaska from tomographic studies (Zhao and Pulpan, 1995) is estimated to be 45-55 km, and their slab location indicates that the zone of relatively small-magnitude seismicity shown in this report is occurring near the top of the slab. Using Puget Sound historic Mw 6 slab earthquakes as an analogue, future large intraslab earthquakes beneath the site are likely to stop at the top of the slab, but extend deeper into the slab rather than be confined to the thin zone of the upper slab based on small magnitude seismicity data that indicates otherwise as shown in this report.

Comparisons to the FCL (2012) PSHA results for this updated intraslab source model show small variations at PHA and 1.0 second spectral acceleration response, indicating that the Wesson et al. (2007) model gives similar results, at least for these response periods, as long as the same M_{max} value is used.

The PSHA results indicate negligible sensitivity to the model parameters correlation distance used to develop occurrence rate grids and ± 2 sigma variations in depth measures from the site to the slab. It is perhaps fortuitous that the Wesson et al. (2007) uniform slab depth of 60 km is very close to the distance from the site to the more refined slab model presented here. The results are also relatively insensitive to a change in V_{s30} to 1080 m/s (FCL, 2014) from the 800 m/s used in FCL (2012).

In contrast, hazard variations due to M_{max} choices of 7.8 and 8.1 are significant. For the two response periods, at a 10,000 year return period, ground motion increases of about 25% and 50% are indicated, respectively. However, due to the paucity of ground motion records for magnitudes above 7.5, magnitude scaling of ground motions in the GMPEs above Mw 7.5 is highly uncertain, and warrants further investigation.

Preliminary investigations into historical occurrence of the largest earthquake magnitudes for worldwide subduction zones indicate that an upper bound value for future slab M_{max} distributions used in the final PSHA analysis is likely to lie between 8.0 and 8.5. As noted in Section 5.0, however, many of the large events in the 100 – 400 km depth range occurred before reliable magnitudes and depth calculations were available, and there is significant uncertainty in global earthquake catalogues regarding the characterization of large events at depths less than 100 km, but still down dip from the location of interface rupture. In other words, it is not clear for many of these events whether they occurred on the plate interface or within the slab.

The Okal (2005) analysis indicates that the 1906 Aleutians event occurred at about 50 km depth, and was not a plate interface earthquake. His magnitude estimate of M_w 8.3 – 8.4 is consistent with earlier magnitude estimates. The moment tensor solution for this event, however, indicates that it may not have occurred within the downgoing slab, but in the overriding plate above the slab, as a result of oblique subduction in this part of the arc. This may preclude this type of event from occurring in the Watana site area, where subduction is much more perpendicular to the plate boundary.

The Okal (2005) and Geller and Kanamori (1977) studies also highlight the fact that surface wave magnitudes of deep events in the worldwide catalog, in particular the 1916 Fox Islands event located at 170 km depth with a listed M_s of 7.4, may have a higher moment magnitude. Since the PSHA is based on moment magnitudes, this distinction is important.

It is recommended that further investigations into the 1916 Fox Islands and 1906 Rat Islands earthquakes be conducted. If sufficient seismograms exist, a study of the 1916 event similar to the Okal (2005) analysis of the Rat Islands event would be important in refining its magnitude, location, and depth, as well as producing a focal mechanism. Investigations into whether the 1906 earthquake was a slab event or not, and whether oblique subduction played a dominant role in its occurrence, are important to judging the possibility of such an event occurring beneath the Watana site, where oblique subduction is minimal.

Another factor specific to the Watana site is that it lies above the McKinley Block, which shows evidence of being physically detached from the Kenai Block, and fragmented at depths below about 90 km. If it is detached and moving independently, available physical volume considerations may place a limit on the maximum size earthquake it can support.

For final PSHA hazard calculations at the Watana dam site, further evaluation of the ASZ and worldwide subduction zone data will need to be conducted to develop appropriate weighting of uncertain parameters such as M_{max} . The present evaluations confirm that the M_{max} value of M_w 7.5 used in the FCL (2012) analyses must likely be considered a minimum estimate for a M_{max} distribution. Further evaluations are needed to assess the full range and weights for larger M_{max}



SUSITNA-WATANA HYDRO

Clean, reliable energy for the next 100 years.

ALASKA ENERGY AUTHORITY

AEA11-022

16-1411-TM-042514

estimates and to develop a basis for estimation of an appropriate characterization of M_{max} for the intraslab source for use in deterministic evaluations.

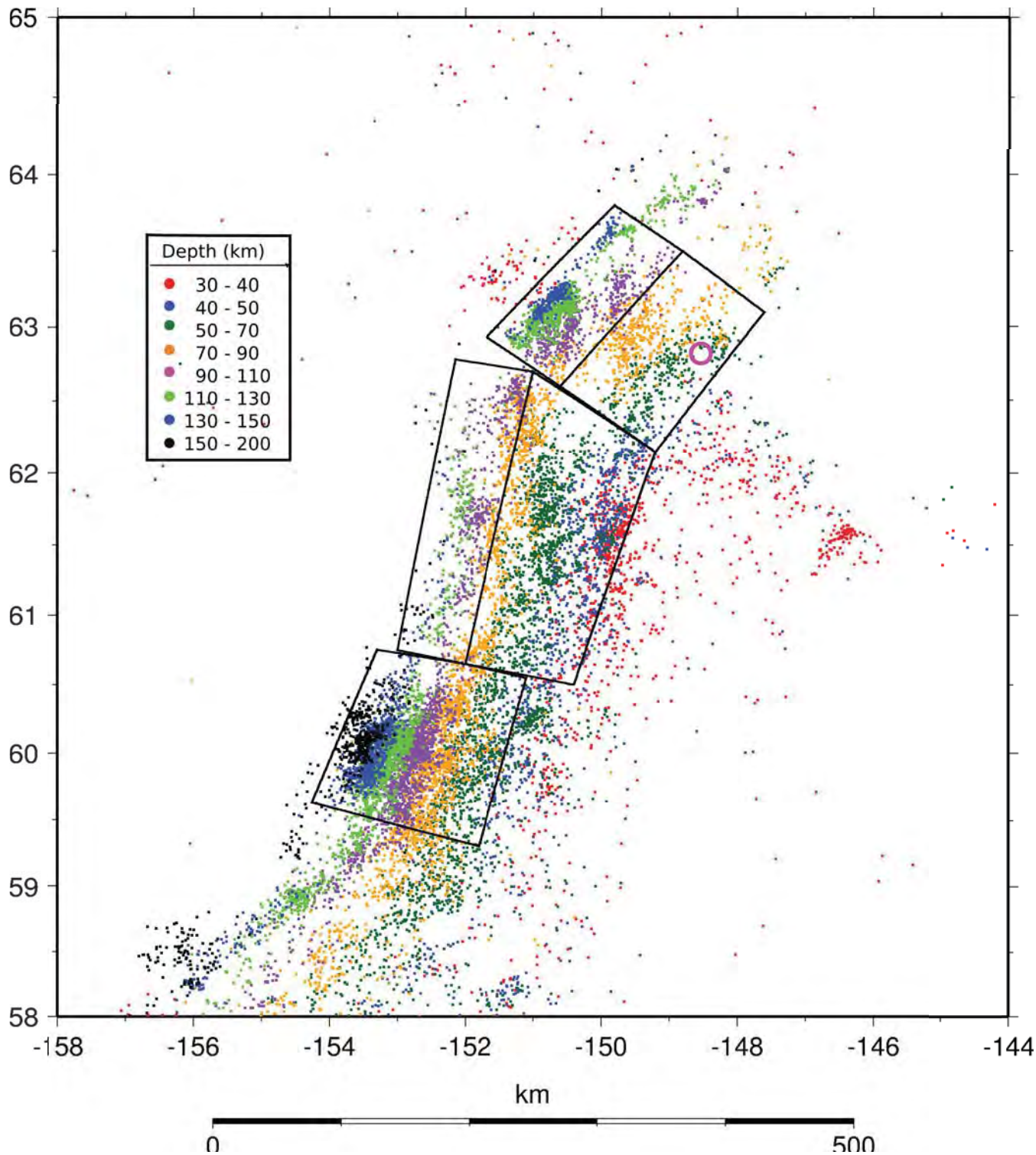
8. REFERENCES

- Abe, K. (1981). Magnitudes of large shallow earthquakes from 1904 to 1980, *Phys. Earth. Planet. Int.*, 27, 72-92.
- Duda, S.J. (1965). Secular seismic energy release in the circum-Pacific belt, *Tectonophysics*, 2, 409-452.
- Engdahl, E.R. (2006). Application of an improved algorithm to high precision relocation of ISC test events, *Phys. Earth. Planet. Int.*, 158, 14-18.
- Frankel, A., C. Mueller, T. Barnhard, D. Perkins, E. Leyendecker, N. Dickman, S. Hanson, and M. Hopper (1996). National seismic-hazard maps: documentation June 1996, U.S. Geological Survey Open-File Report 96-532.
- Frohlich, C. (1998). Does maximum earthquake size depend on focal depth?, *Bulletin of the Seismological Society of America*, Vol. 88, No. 2, 329-336.
- Frohlich, C. (2006). *Deep Earthquakes*, Cambridge University Press, 573 pp.
- Fugro Consultants, Inc. (FCL) (2012). Seismic Hazard Characterization and Ground Motion Analyses for Susitna-Watana Dam Site, NTP 6, Technical Memorandum No.4.
- Fugro Consultants, Inc. (FCL) (2014). Watana Seismic Network Station Vs30 Measurements, NTP 16, Technical Memorandum No. 14-07.
- Fuis, G.S., T.E. Moore, G. Plafker, T.M. Brocher, M.A. Fisher, W.D. Mooney, W.J. Nokleberg, R.A. Page, B.C. Beaudoin, N.I. Christensen, A.R. Levander, W.J. Lutter, R.W. Saltus, and N.A. Ruppert (2008). Trans-Alaska Crustal Transect and continental evolution involving subduction underplating and synchronous foreland thrusting, *Geology*, 36; no. 3, 267-270.
- Gardner, J.K., and L. Knopoff (1974). Is the sequence of earthquakes in southern California, with aftershocks removed, Poissonian?, *Bulletin of the Seismological Society of America*, 64, 1363-1367.
- Geller, R.J., and H. Kanamori (1977). Magnitudes of great shallow earthquakes from 1904 to 1952, *Bulletin of the Seismological Society of America*, 67, 587-598.
- Gutenberg, B. and C.F. Richter (1954). *Seismicity of the earth and associated phenomena*, 2nd Ed. Princeton University Press, Princeton, NJ, 301 pp.
- Hanks, T.C., and H. Kanamori (1979), A moment magnitude scale, *Journal of Geophysical Research*, 84, B5, 2348-2350.

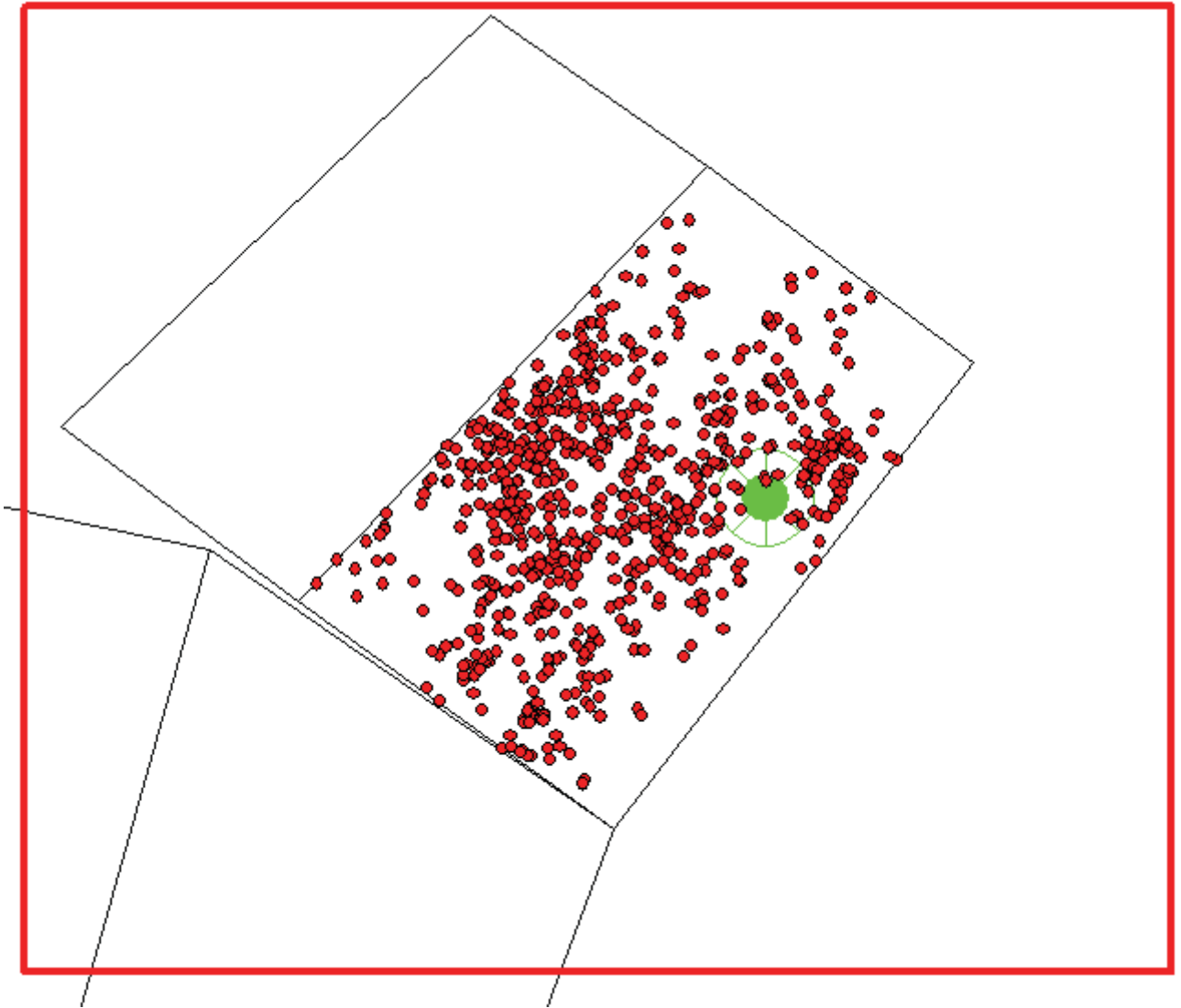
-
- Hayes, G.P., D.J. Wald, and R. L. Johnson (2012). Slab1.0: A three-dimensional model of global subduction zone geometries, *Journal of Geophysical Research*, 117, B01302, doi:10.1029/2011JB008524.
- Huang, W., E.A. Okal, G. Ekstrom, and M.P. Salganik (1997). Centroid moment tensor solutions for deep earthquakes predating the digital era: the World-Wide Standardized Seismograph Network dataset (1962-1976), *Phys. Earth. Planet. Int.*, 99, 121-129.
- Huang, W., E.A. Okal, G. Ekstrom, and M. P. Salganik (1998). Centroid moment tensor solutions for deep earthquakes predating the digital era: The historical dataset (1907-1961), *Phys. Earth.*
- Ichinose, G., H. Thio, and P. Somerville (2006), Moment tensor and rupture model for the 1949 Olympia, Washington, earthquake and scaling relations for Cascadia and global intraslab earthquakes, *Bulletin of the Seismological Society of America*, 96, 1029-1037.
- Kanamori, H. (1977). The energy release in great earthquakes, *Journal of Geophysical Research*, 82, 2981-2987.
- Janiszewski, H., G. Abers, D. Shillington, and J. Calkins (2013), Crustal structure along the Aleutian island arc: New insights from receiver functions constrained by active-source data, *Geochemistry, Geophysics, Geosystems*, 14, n. 8, 2977–2992.
- LaForge, R., and E.R. Engdahl (1979), Tectonic implications of seismicity in the Adak Canyon region, central Aleutians, *Bulletin of the Seismological Society of America*, 69, 1515-1532.
- McCann, W.R., J.W. Dewey, A. Murphy, and S. Harding (1982), A large normal-fault earthquake in the overriding wedge of the Lesser Antilles subduction zone: the earthquake of 8 October 1974, *Bulletin of the Seismological Society of America*, 72, 2267-2283.
- Okal, E. A. (2005). A re-evaluation of the great Aleutian and Chilean earthquakes of 1906 August 17, *Geophys. J. Int.*, 161, 268-282.
- Ratchkovski, N.A. and R.A. Hansen (2002). New evidence for segmentation of the Alaska Subduction Zone, *Bulletin of the Seismological Society of America*, 92, 1754-1765.
- Richter, C.F. (1958). *Elementary Seismology*, W.H. Freeman, San Francisco.
- Ruppert, N., and R. Hansen (2002). Temporal and spatial variations of local magnitudes in Alaska and Aleutians and comparison with body-wave and moment magnitudes, *Bulletin of the Seismological Society of America*, 100, 1174-1183.
- Tanioka, Y., L. Ruff, and K. Satake (1995). The great Kurile earthquake of October 4, 1994 tore the slab, *Geophysical Research Letters*, 22, 1661-1664.

-
- Tichelaar, B.W., and L.J. Ruff (1993). Depth of seismic coupling along subduction zones, *Journal of Geophysical Research*, 98, B2, 2017-2037.
- Weichert, D. (1980). Estimation of the earthquake recurrence parameters for unequal observation periods for different magnitudes, *Bulletin of the Seismological Society of America*, 70, 1337-1347.
- Wesson, R. L., Boyd, O. S., Mueller, C. S., Bufe, C. G., Frankel, A. D., Petersen, M. D. (2007). Revision of time-Independent probabilistic seismic hazard maps for Alaska: U.S. Geological Survey Open-File Report 2007-1043.
- Zhao, D., D. Christensen, and H. Pulpan (1995), Tomographic imaging of the Alaska subduction zone, *Journal of Geophysical Research*, 100, B4, 6487-6504.

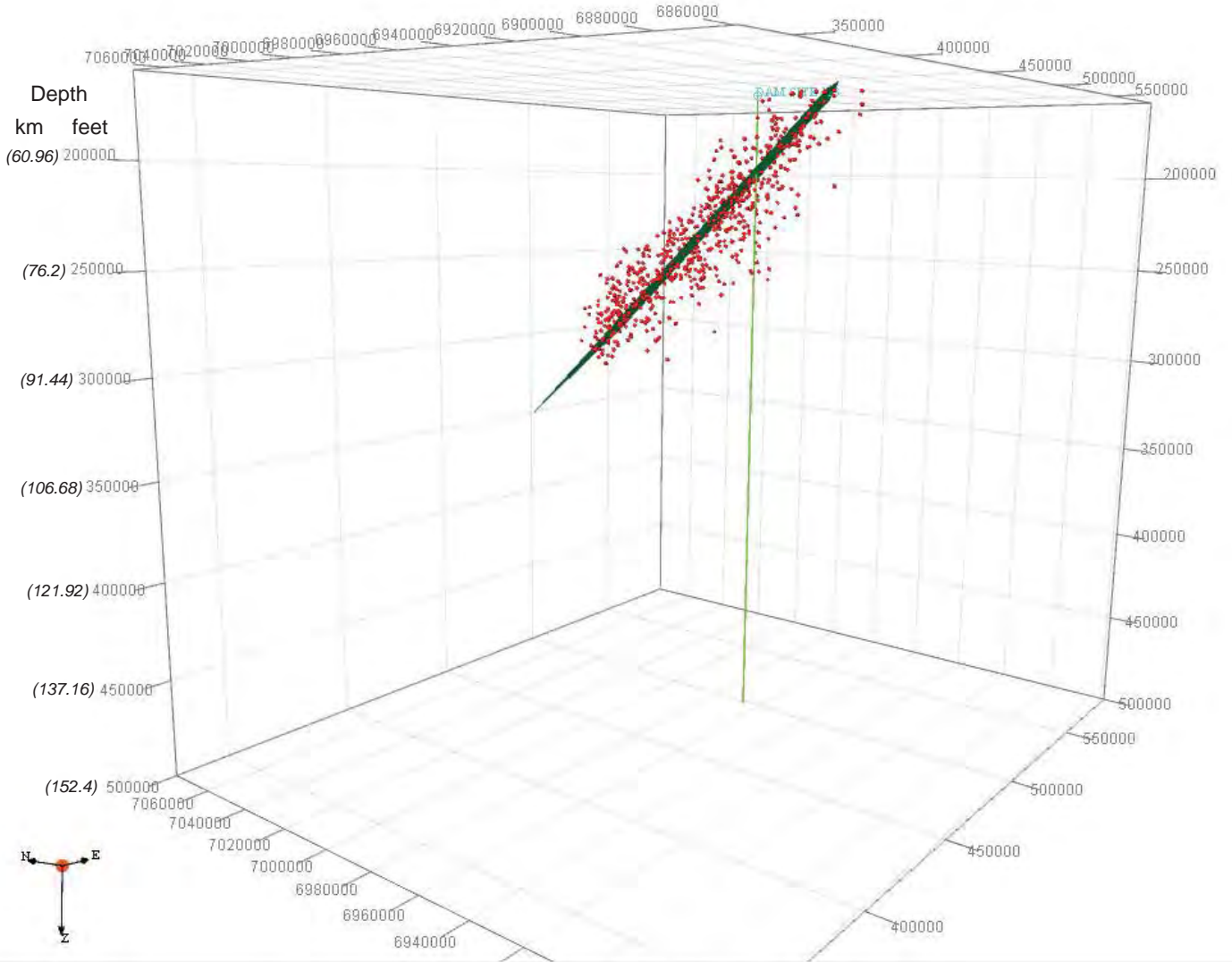
THIS PAGE INTENTIONALLY LEFT BLANK



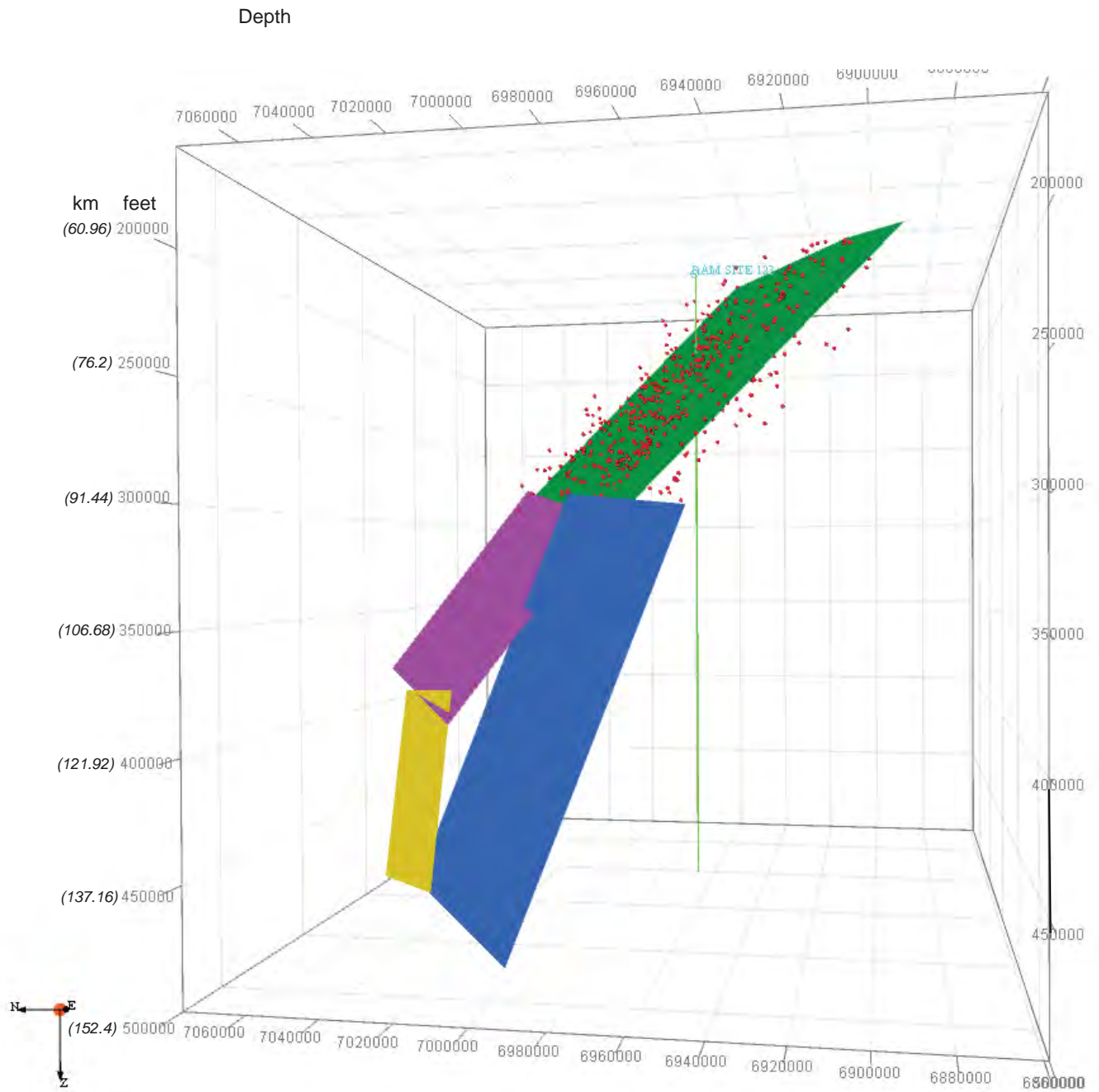
Rectangles are used for identification of slab planes. Magenta circle is Watana dam site.



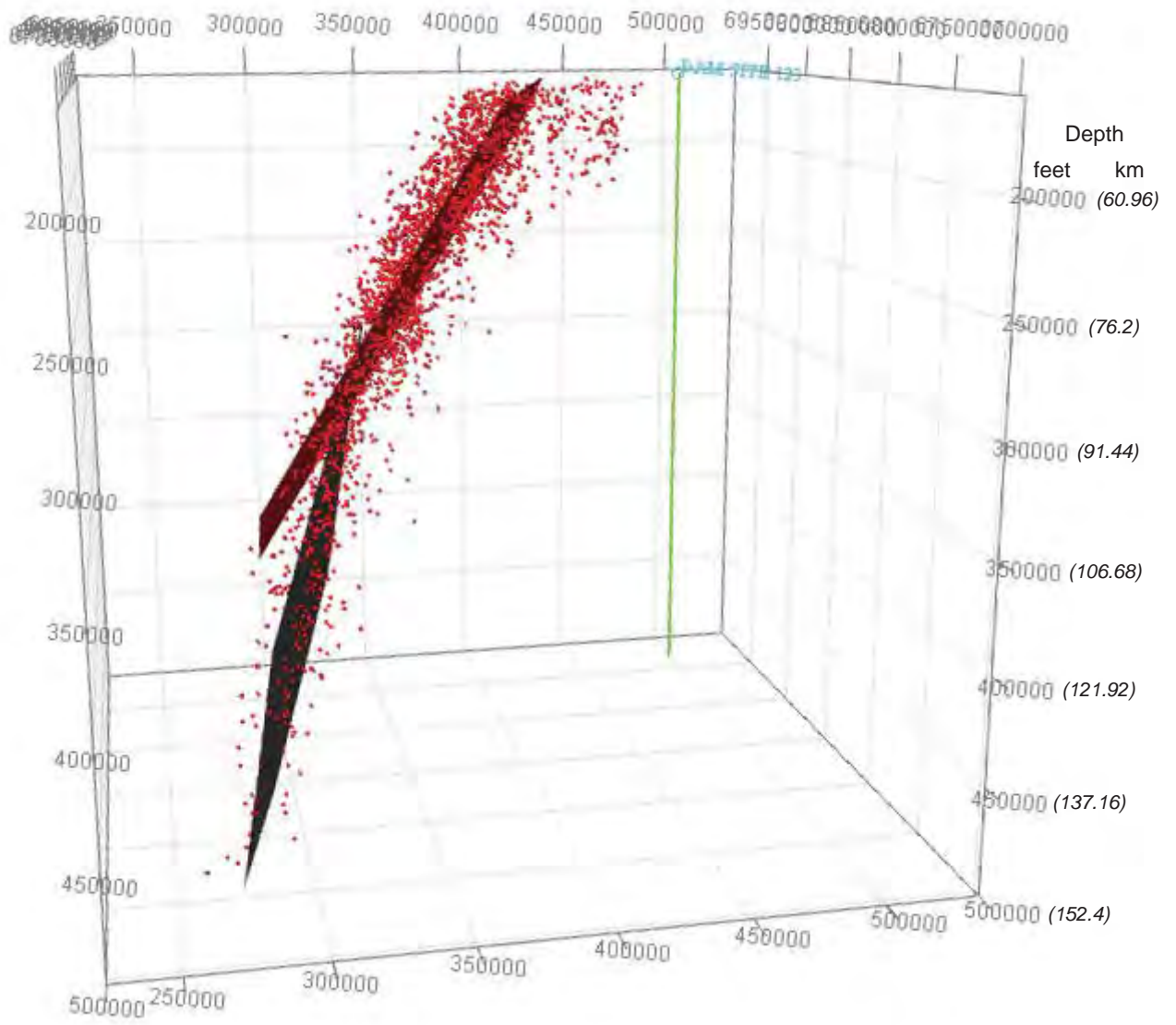
Green circle is Watana site.



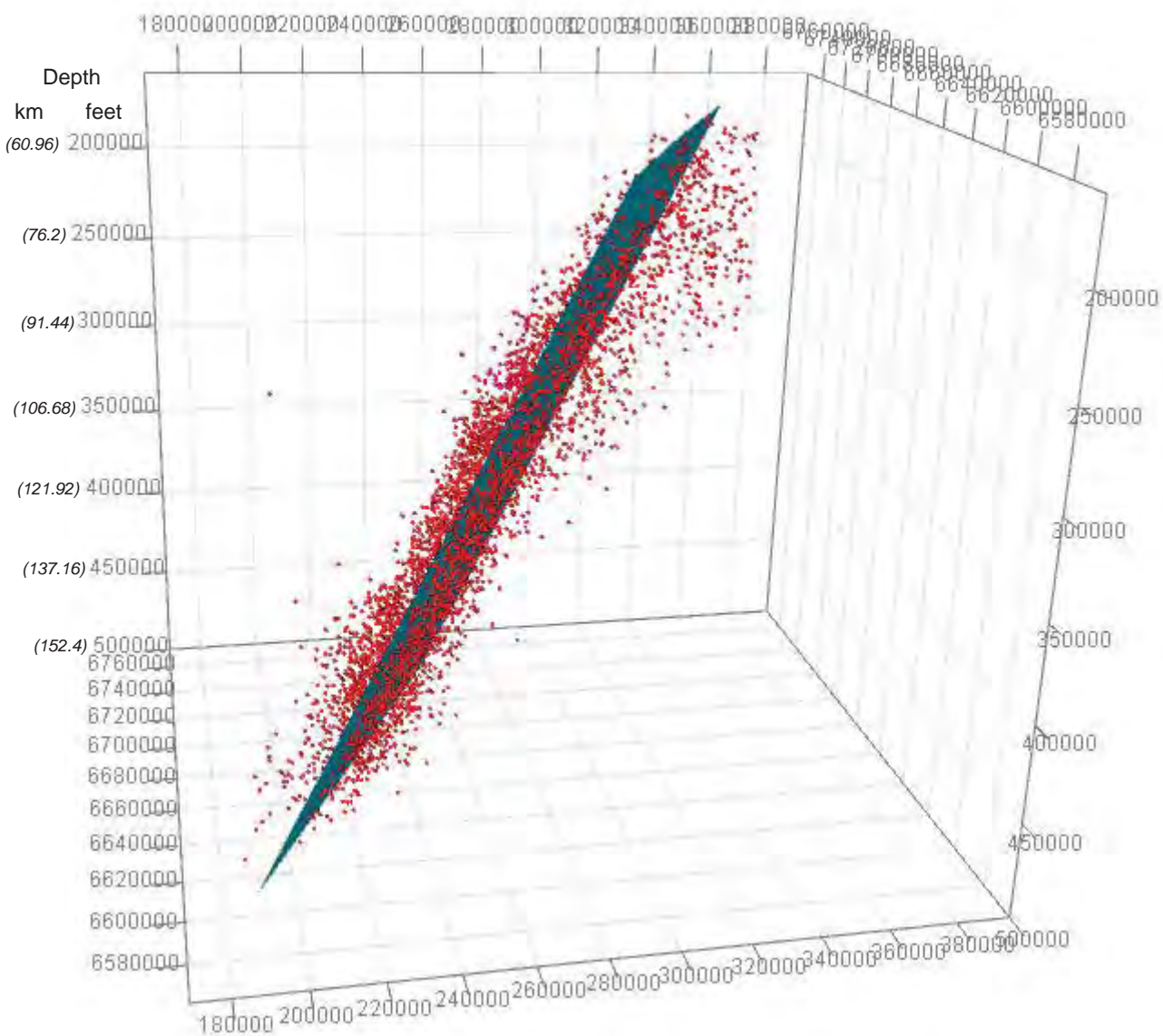
Notes: 1. Black line is plane fit to seismicity.
 2. Green line represents location of Watana site.



View looking NNE



View looking north



View looking north

79_218900_Alaska_Railbel/2189_Lineament Report/04.08.14

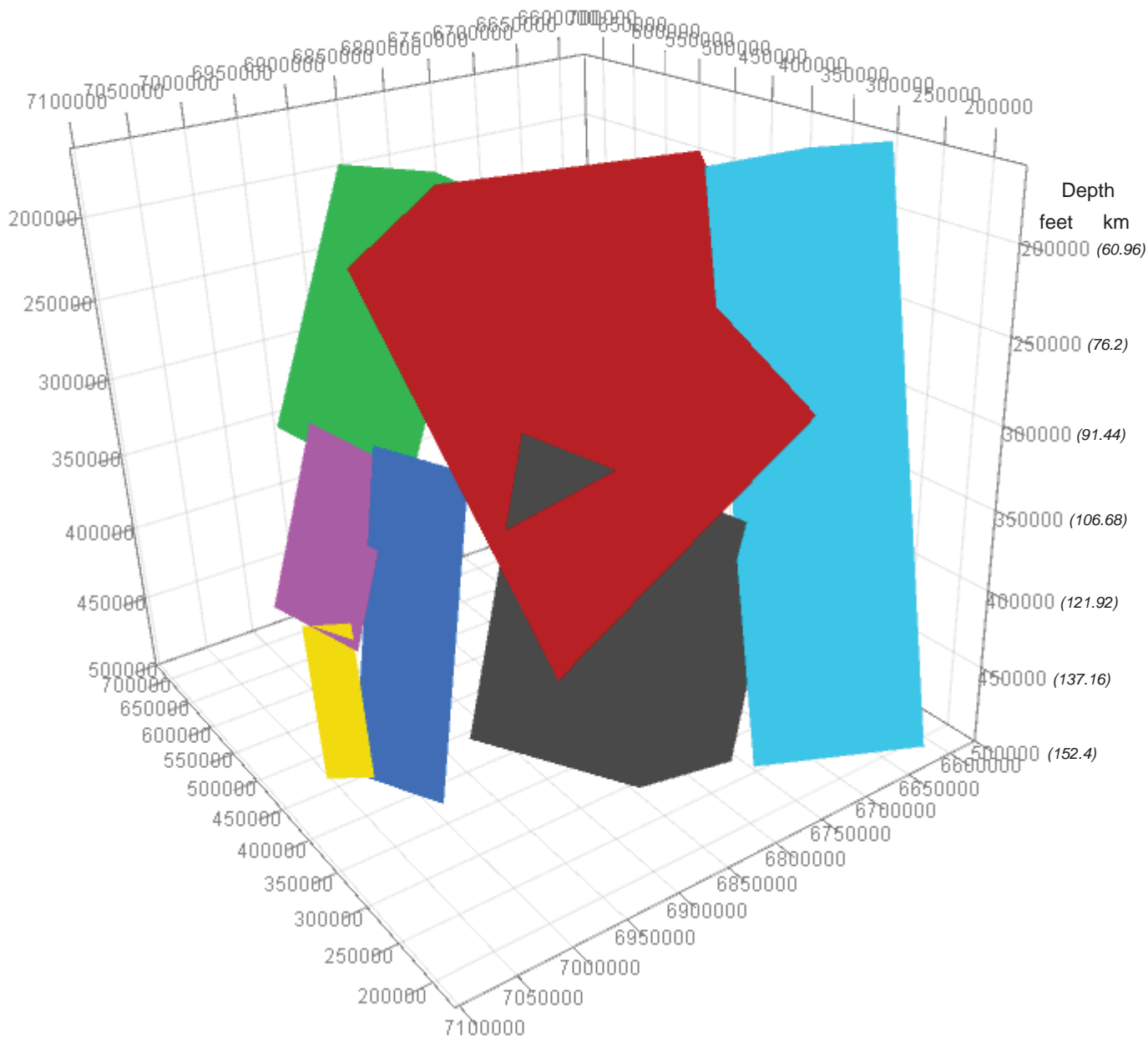


Date 04/08/14



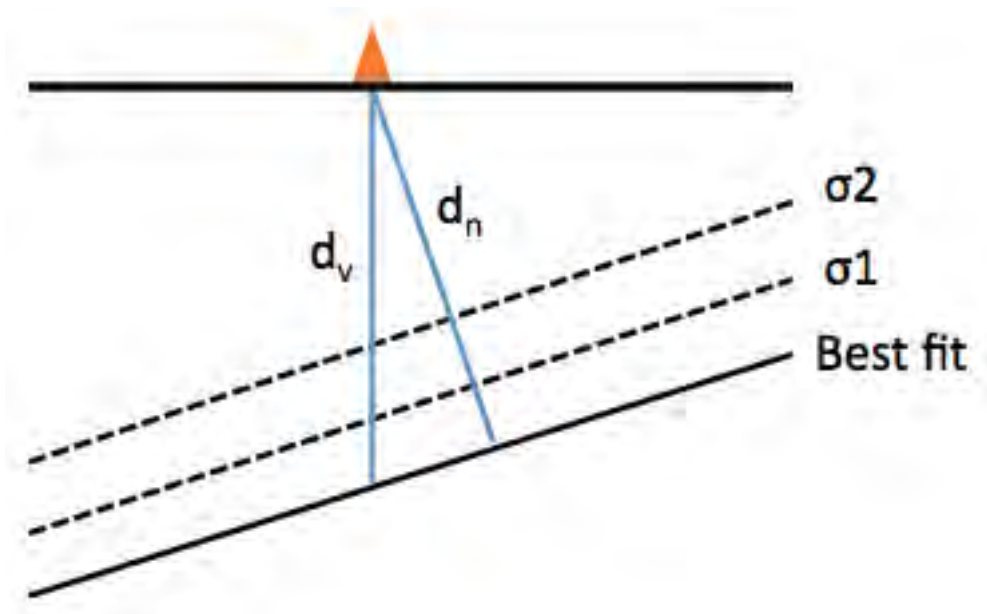
SUSITNA-WATANA HYDROELECTRIC PROJECT
 3D DEPICTION AND FITTED PLANES TO SEISMICITY IN SOUTHERNMOST BOX OF FIGURE 1 (PLANE 7).

FIGURE 6

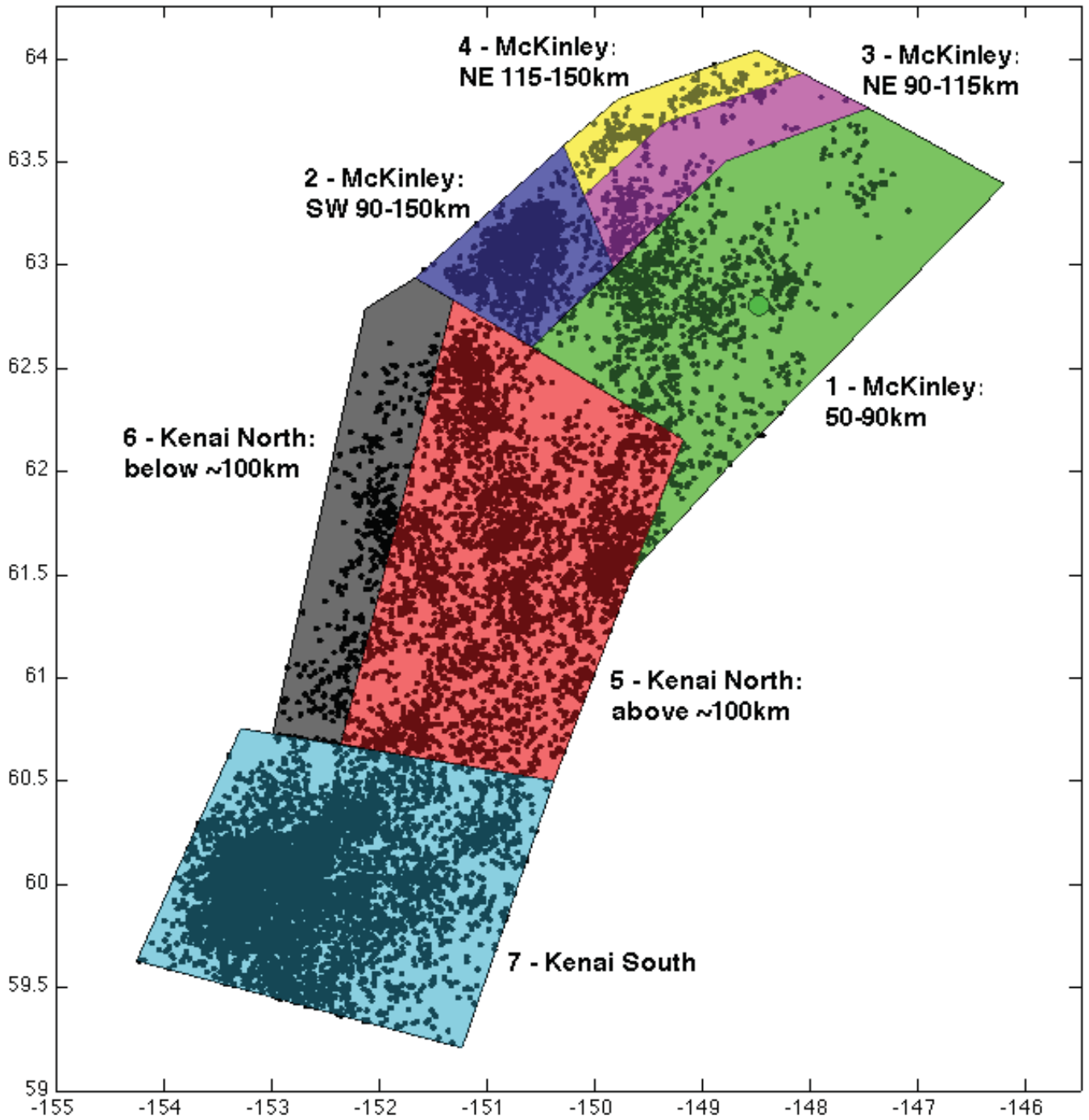


View looking northeast





d_v is hypocentral depth, d_n is distance to rupture.

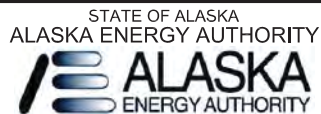


Numbers referenced in Table 2. Green circle in Plane 1 is Watana Dam site.

79_218900_Alaska_Railbel/2189_Lineament_Report/102113



Date 10/21/13

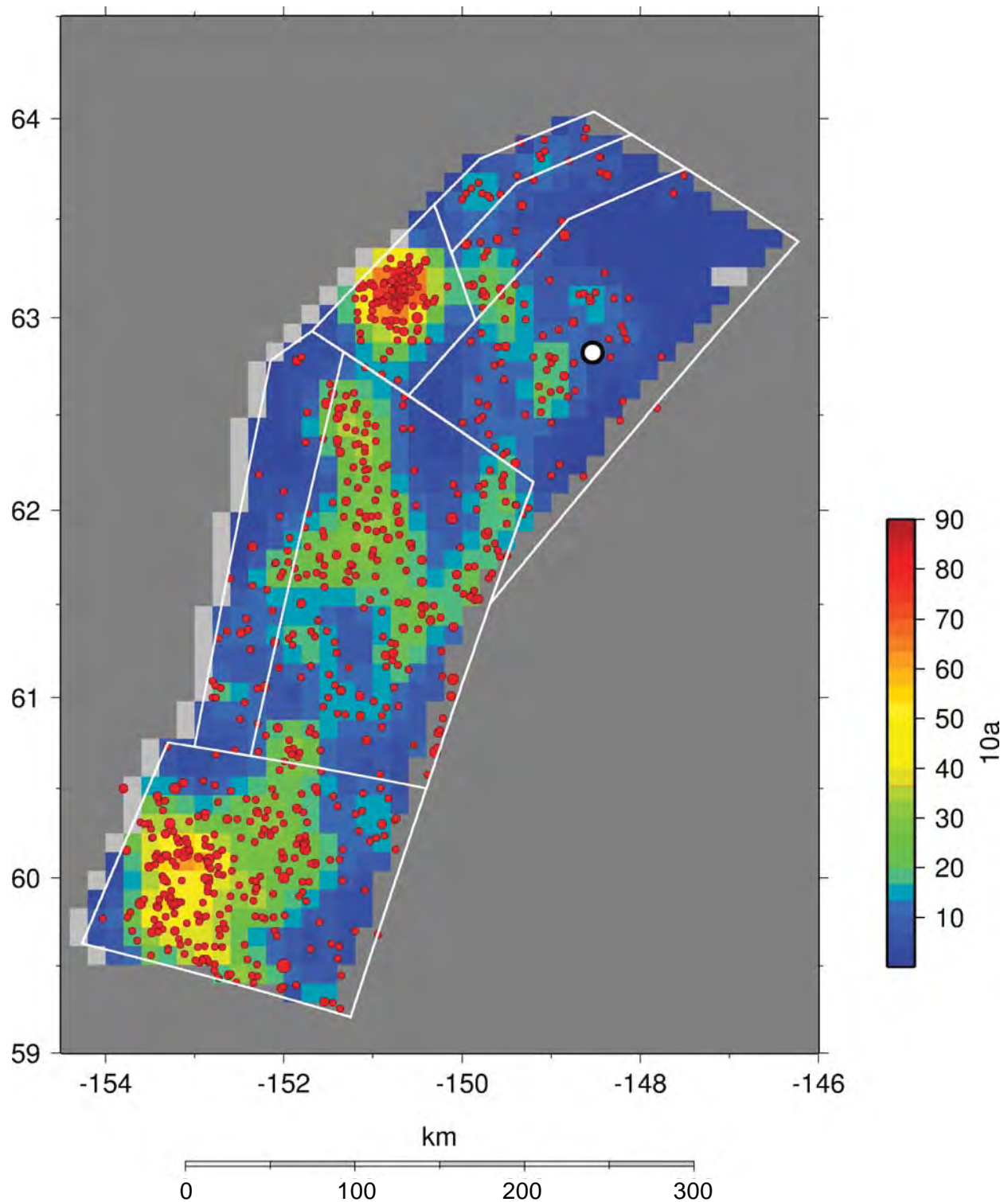


SUSITNA-WATANA HYDROELECTRIC PROJECT

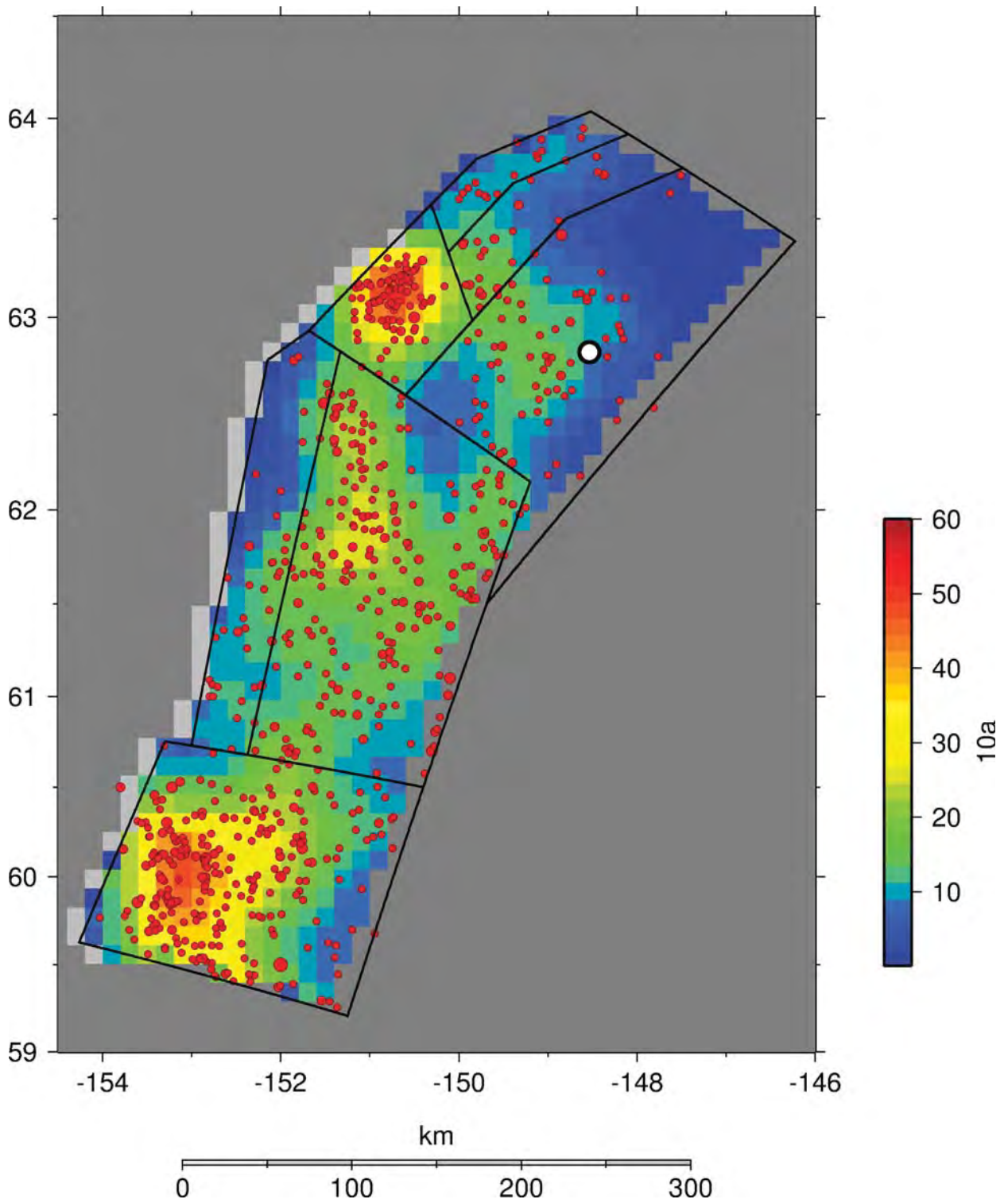
MAP VIEW OF SLAB PLANES

FIGURE

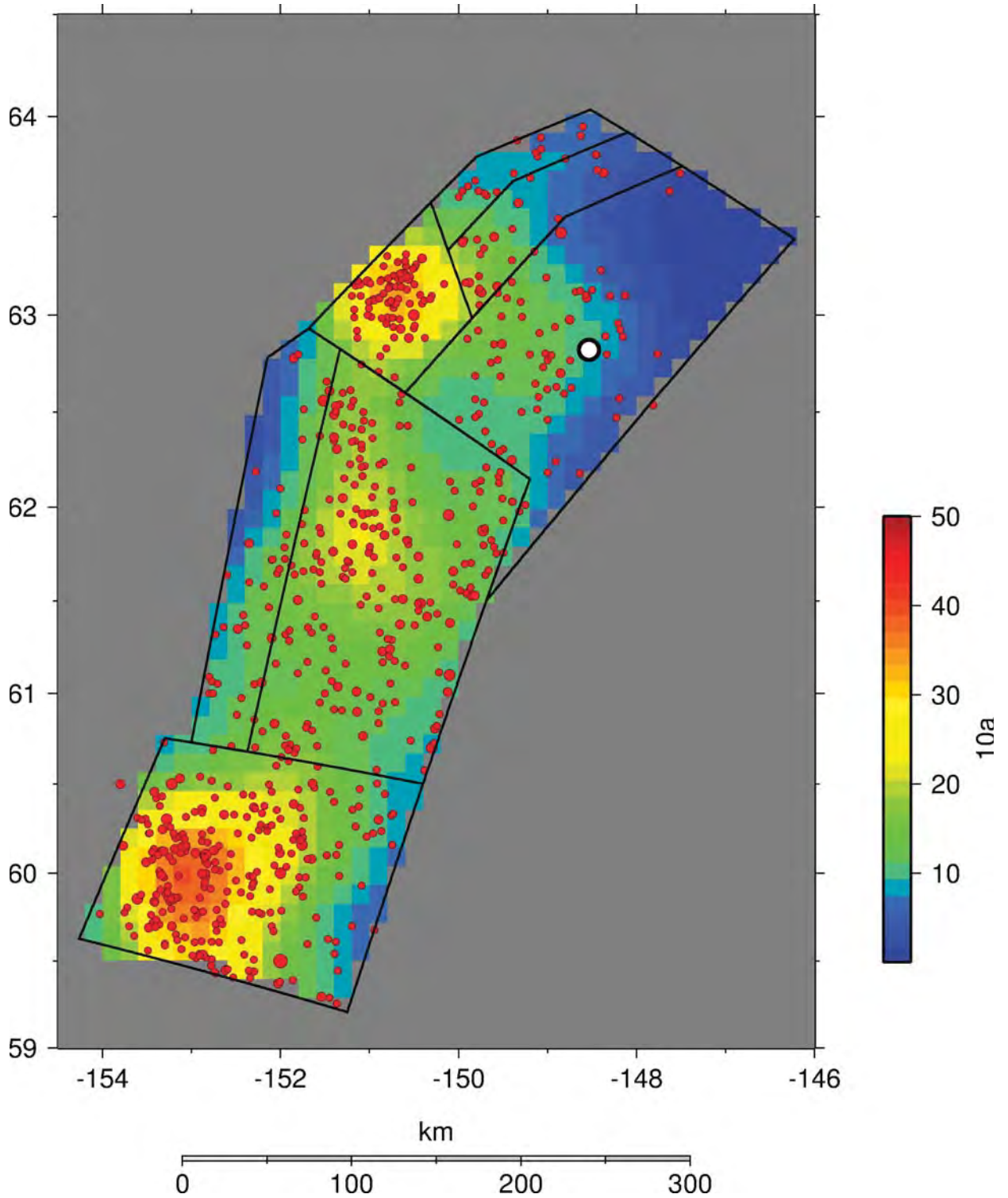
9



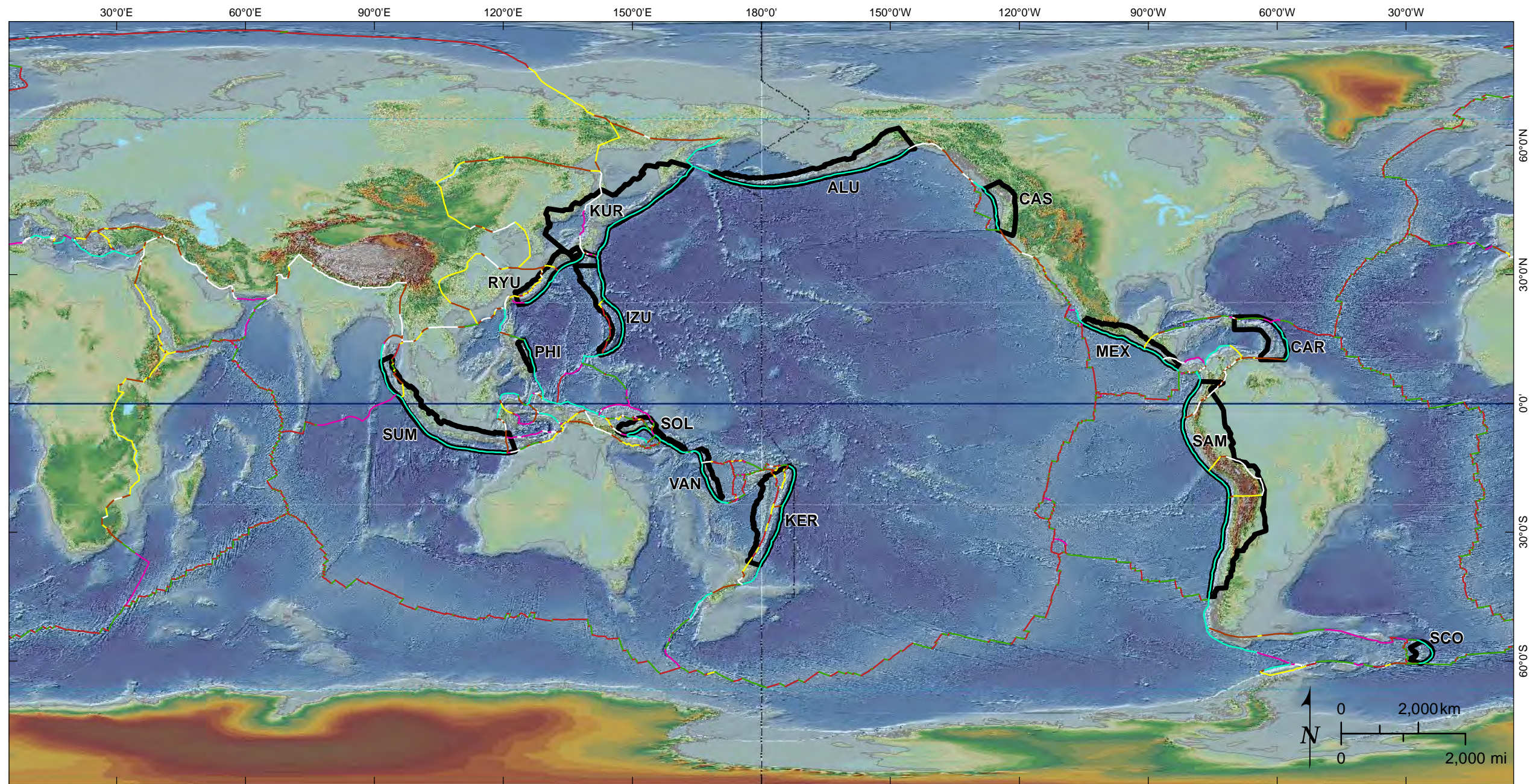
Red dots are earthquakes used to generate the grid. White circle is Watana site.



Red dots are earthquakes used to generate the grid. White circle is Watana site.



Red dots are earthquakes used to generate the grid. White circle is Watana site.



Elevation data from NGDC, 2001.

Explanation

*Tectonic plate boundaries
(from Bird, 2003)*

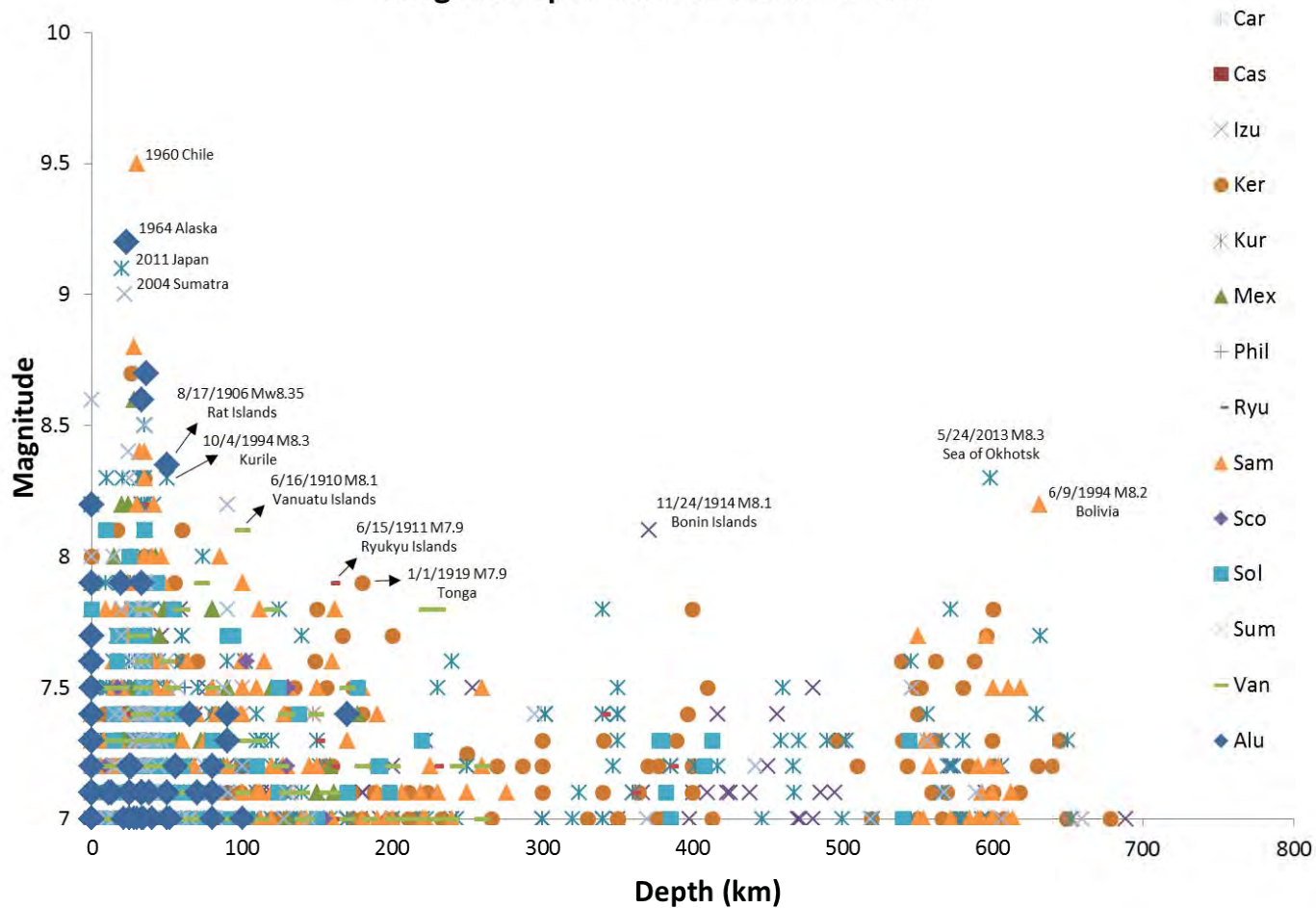
- Subduction boundary
- Continental convergent boundary
- Continental rift boundary
- Continental transform fault
- Oceanic convergent boundary
- Oceanic spreading rift
- Oceanic transform fault

MEX Extent of subduction zone
(from Hayes et al., 2012)

Abbreviaton	Region
ALU	Alaska-Aleutians
CAR	Caribbean-Lesser Antilles
MEX	Central America
CAS	Cascadia
IZU	Izu-Bonin
KER	Kermadec-Tonga
KUR	Kamchatka/Kurilis/Japan

Abbreviaton	Region
PHI	Philippines
RYU	Ryukyu
VAN	Santa Cruz Islands/Vanuatu/Loyalty Islands
SCO	Scotia
SOL	Solomon Islands
SAM	South America
SUM	Sumatra-Java

Mag vs. Depth - All Subduction Zones



79_218900_Alaska_Railbel/2189_Lineament Report/04.14.14



Date 04/14/14

STATE OF ALASKA
ALASKA ENERGY AUTHORITY
ALASKA
ENERGY AUTHORITY

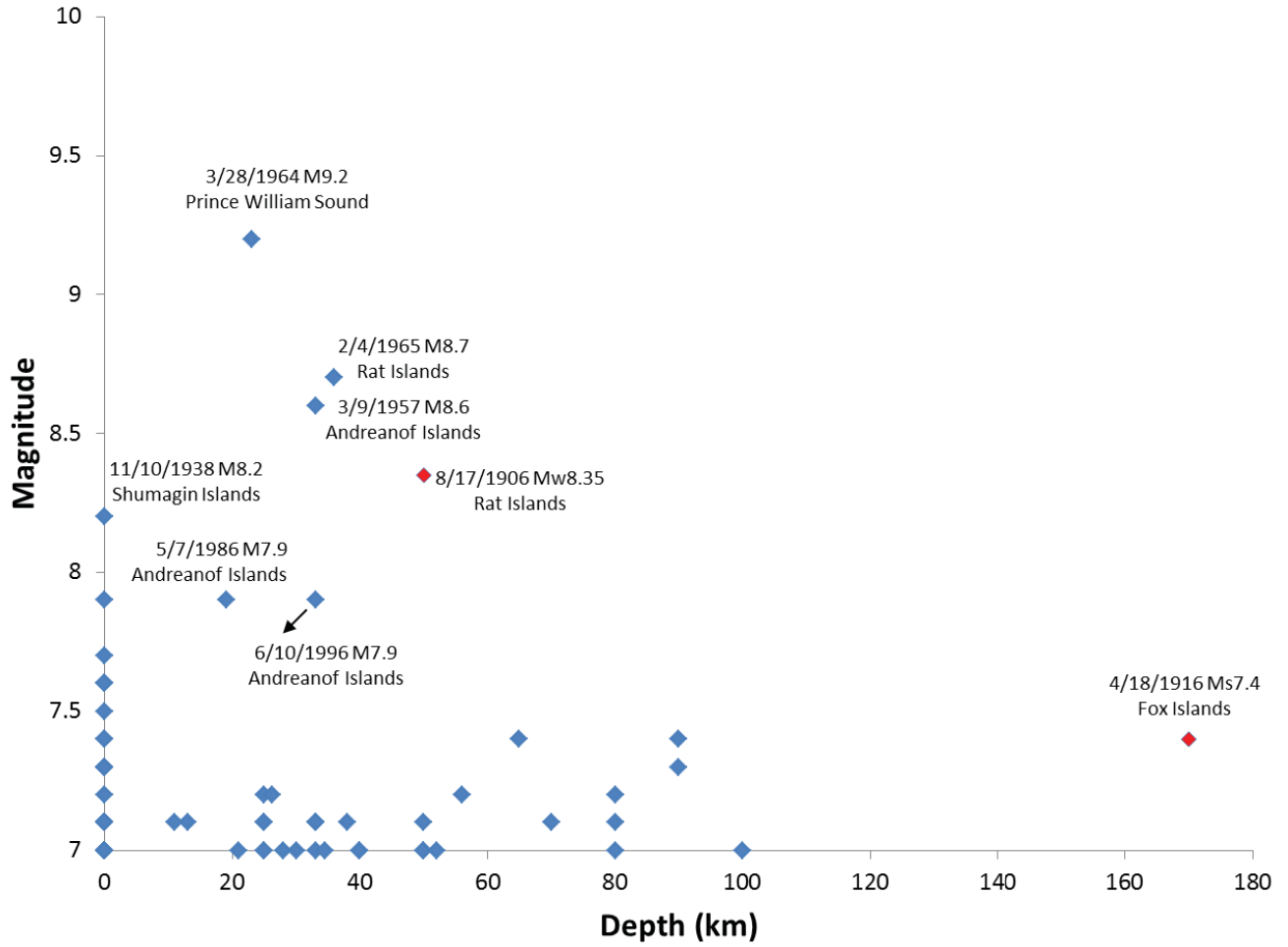
SUSITNA-WATANA HYDROELECTRIC PROJECT

SUMMARY MAGNITUDE VS. DEPTH
PLOT OF ALL SUBDUCTION ZONES

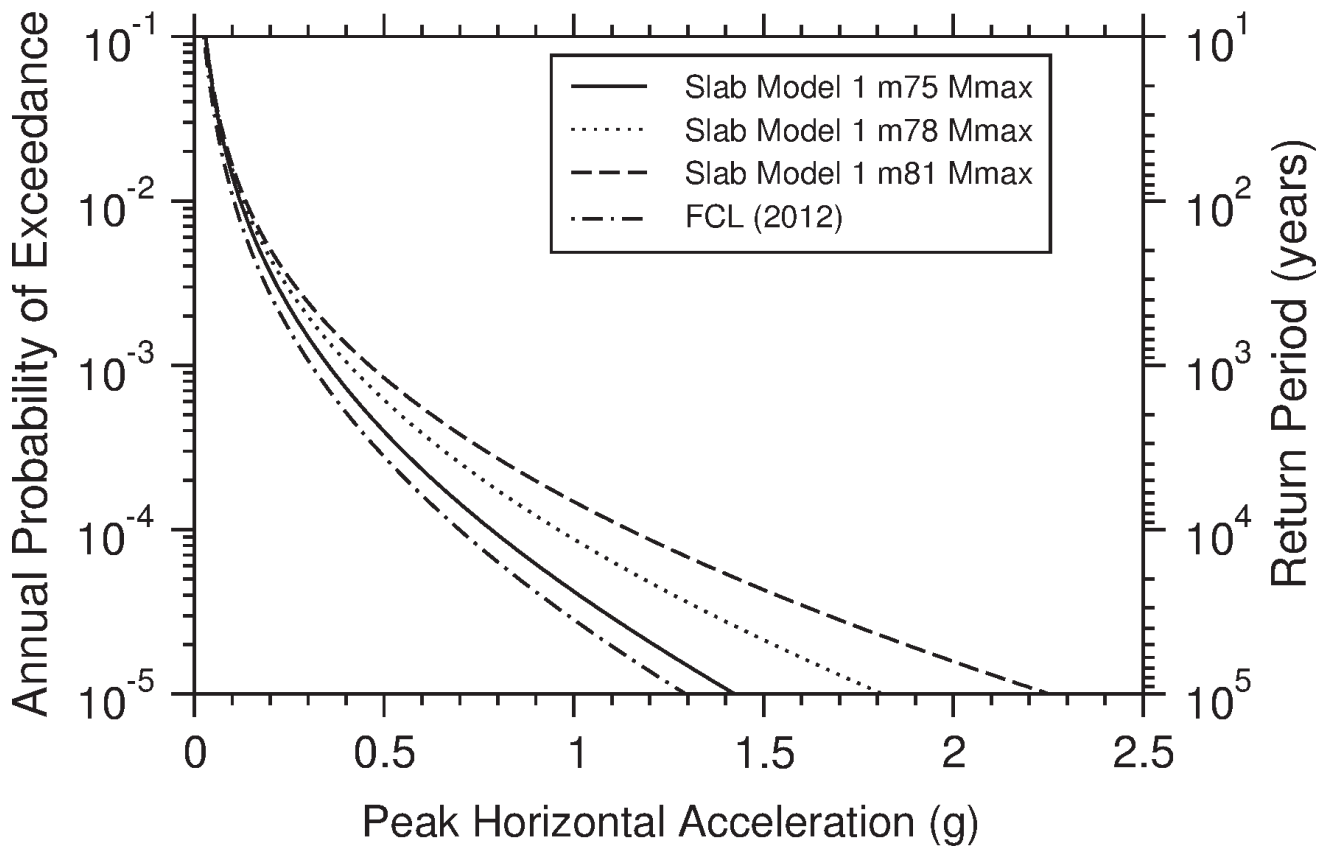
FIGURE

14

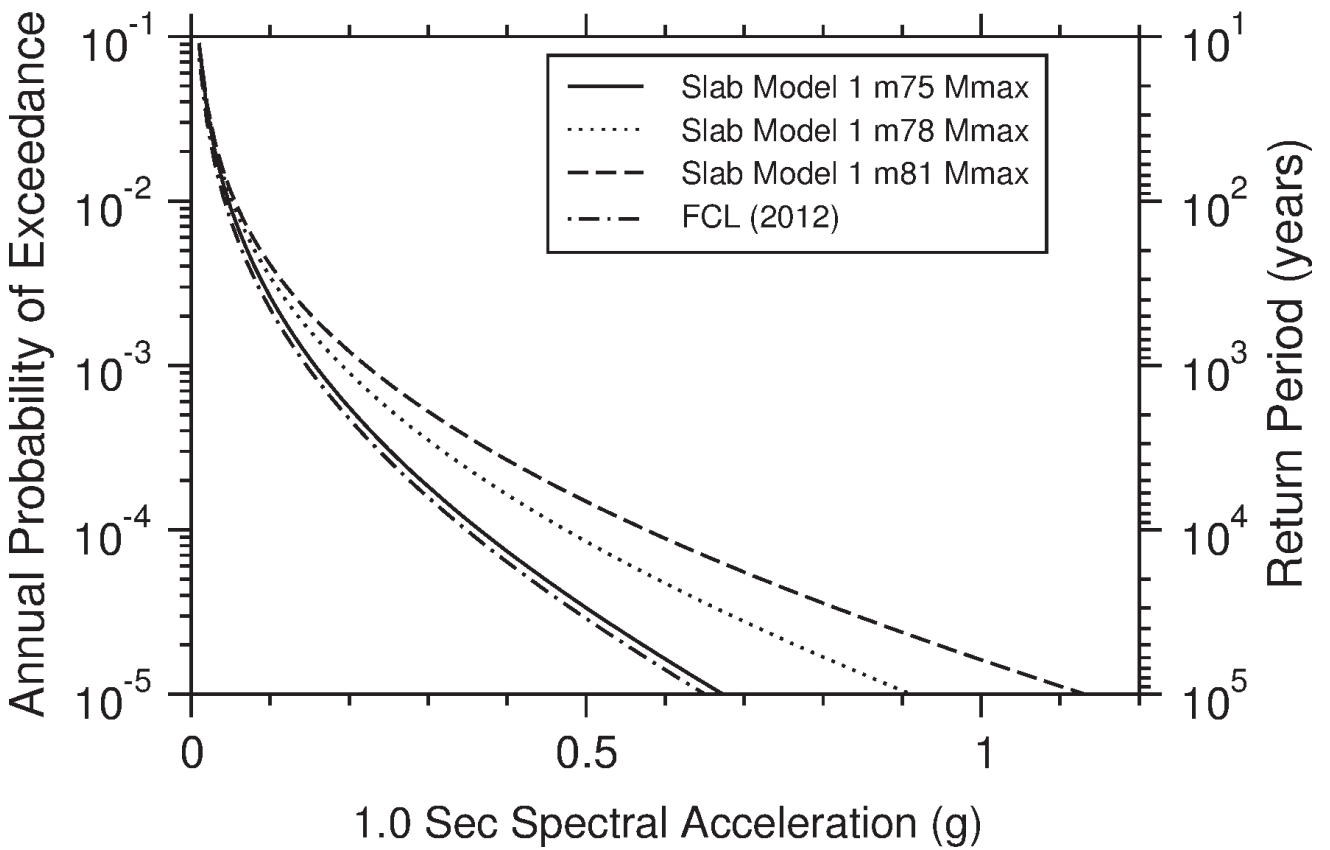
Mag vs. Depth - Alaska-Aleutians Subduction Zone



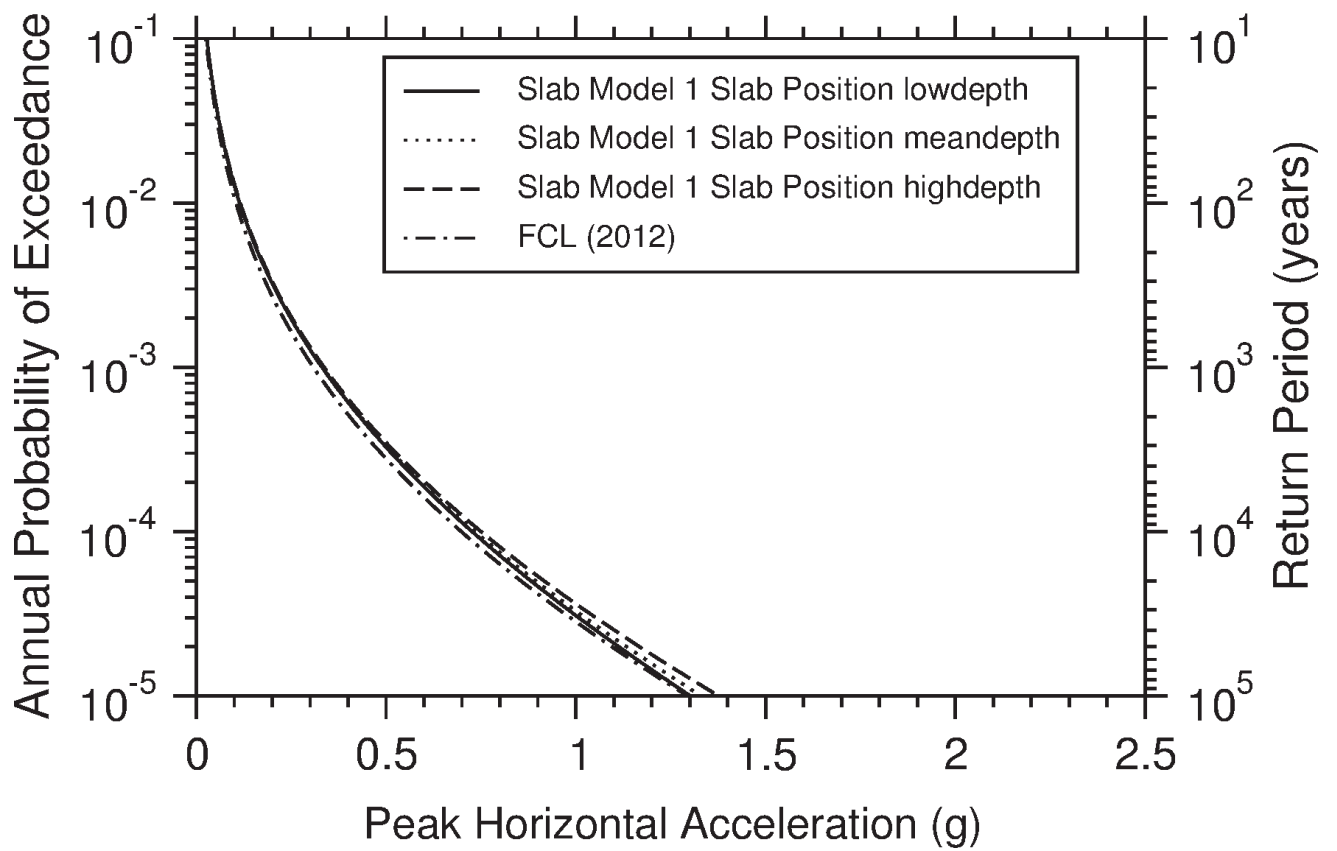
Mmax Sensitivity



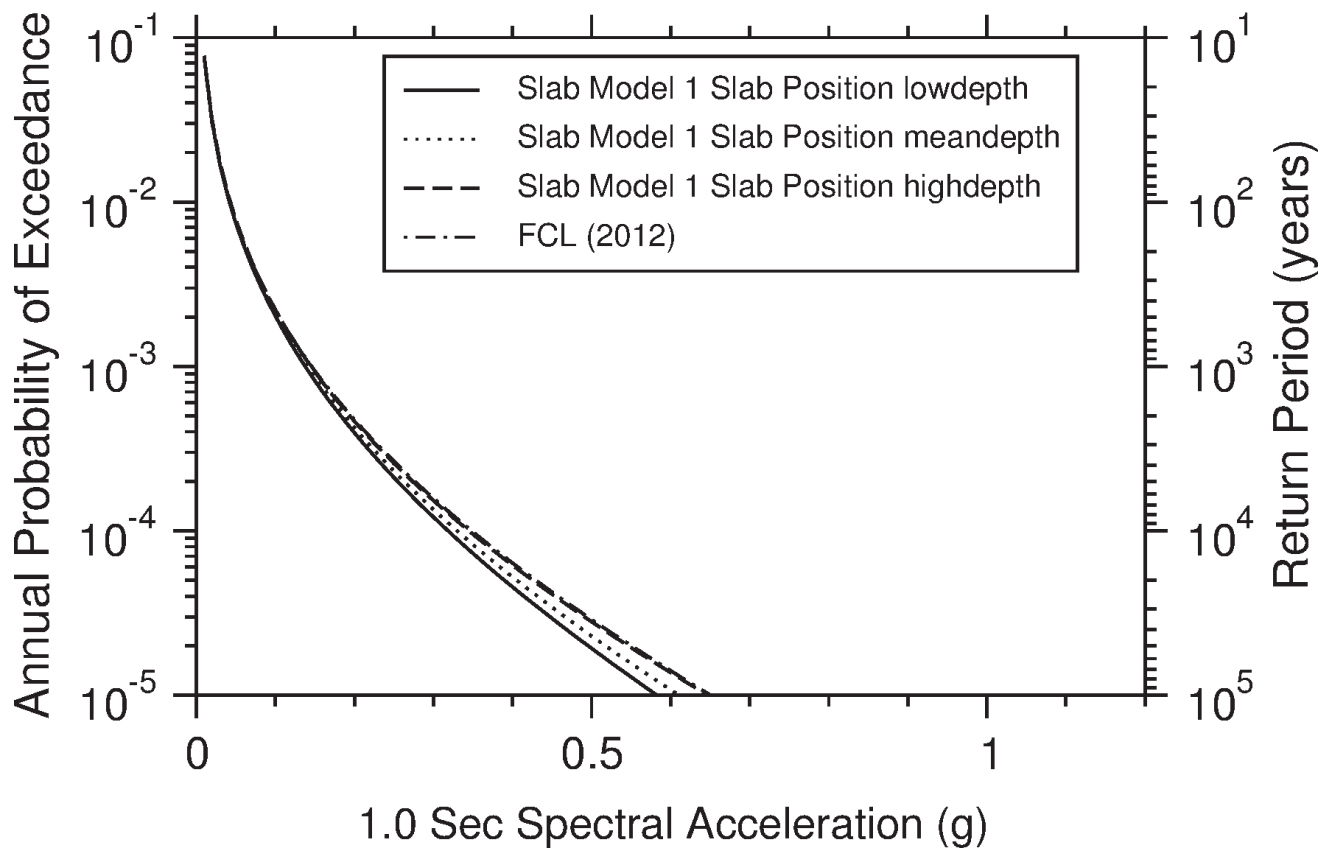
Mmax Sensitivity



Slab Position Sensitivity

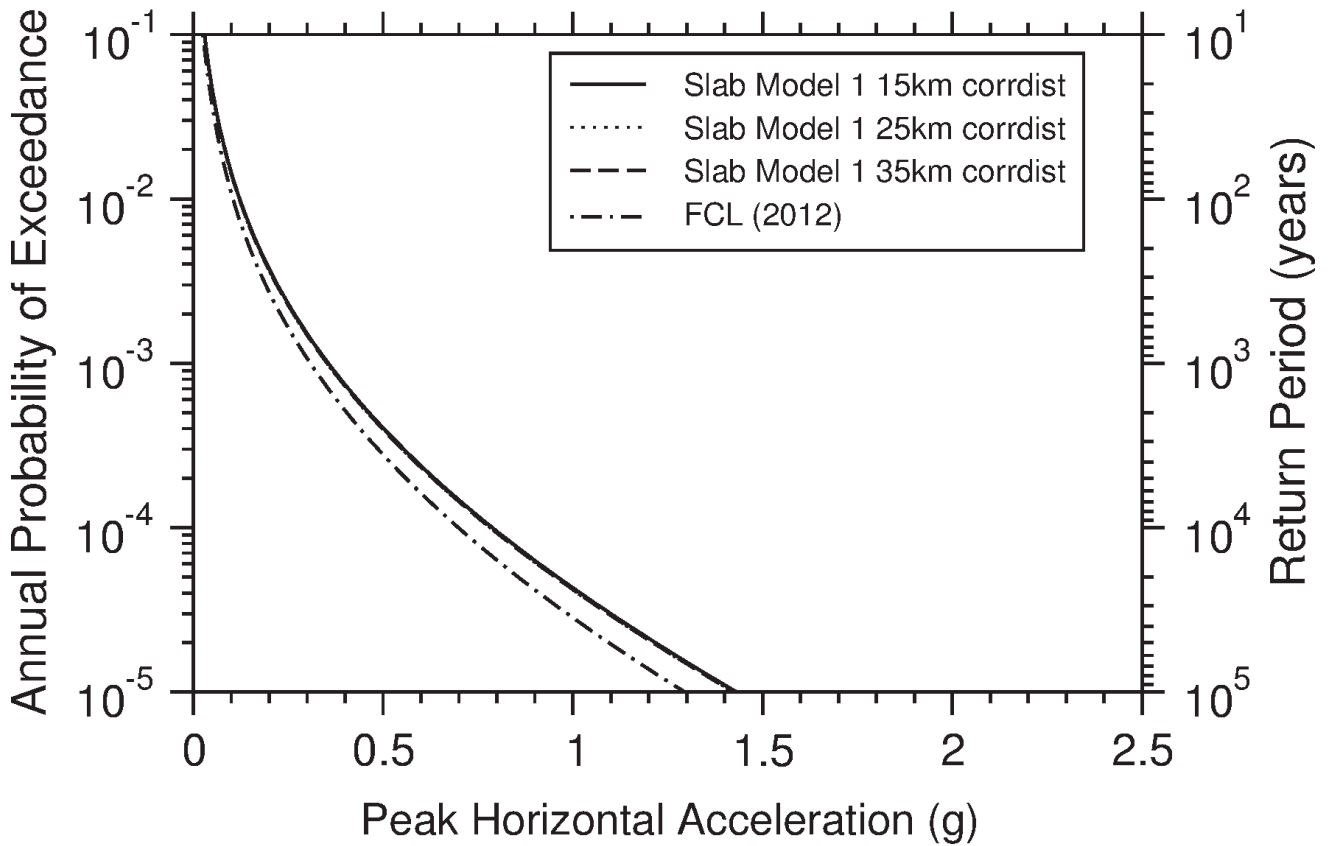


Slab Position Sensitivity

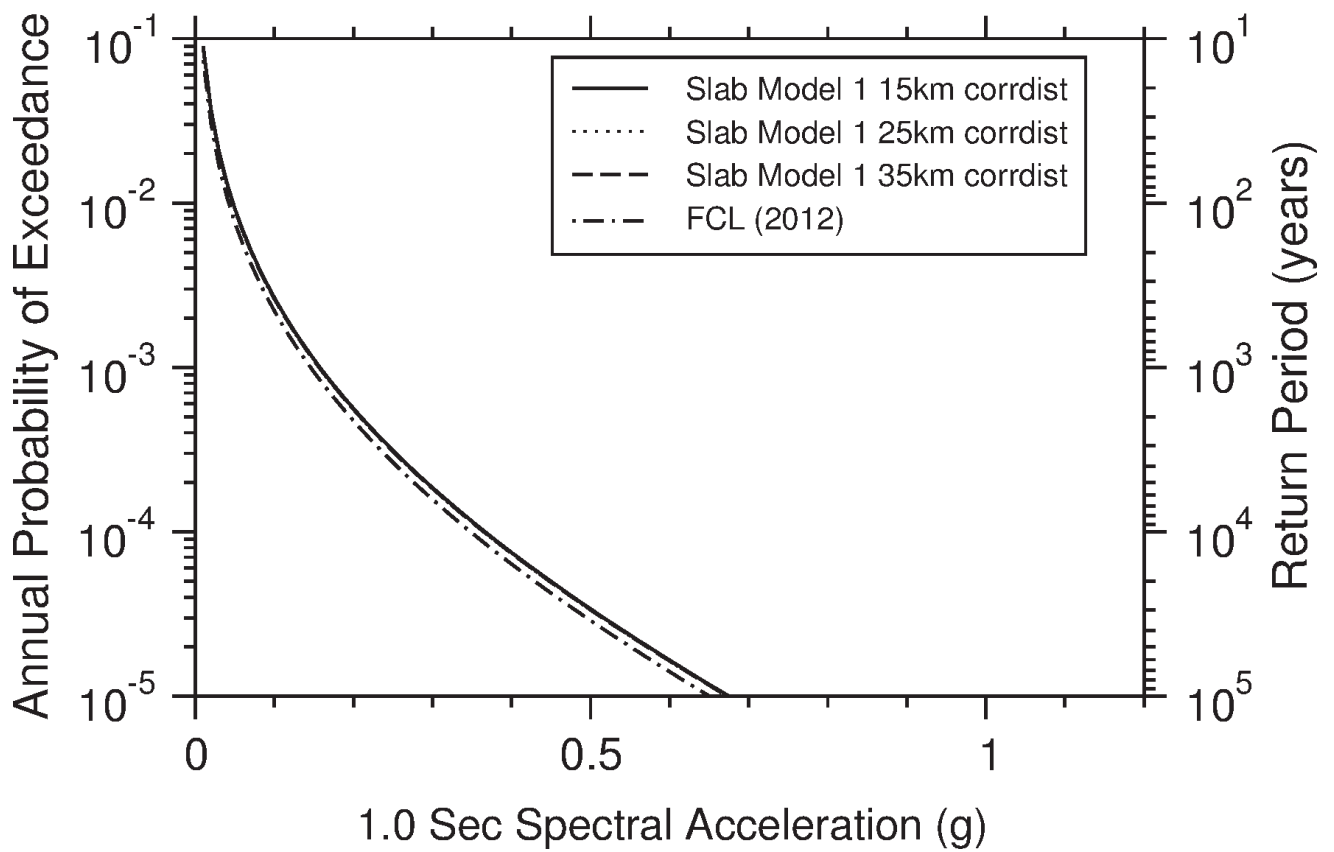


79_218900_Alaska_Railbel/2189_Lineament Report/102113

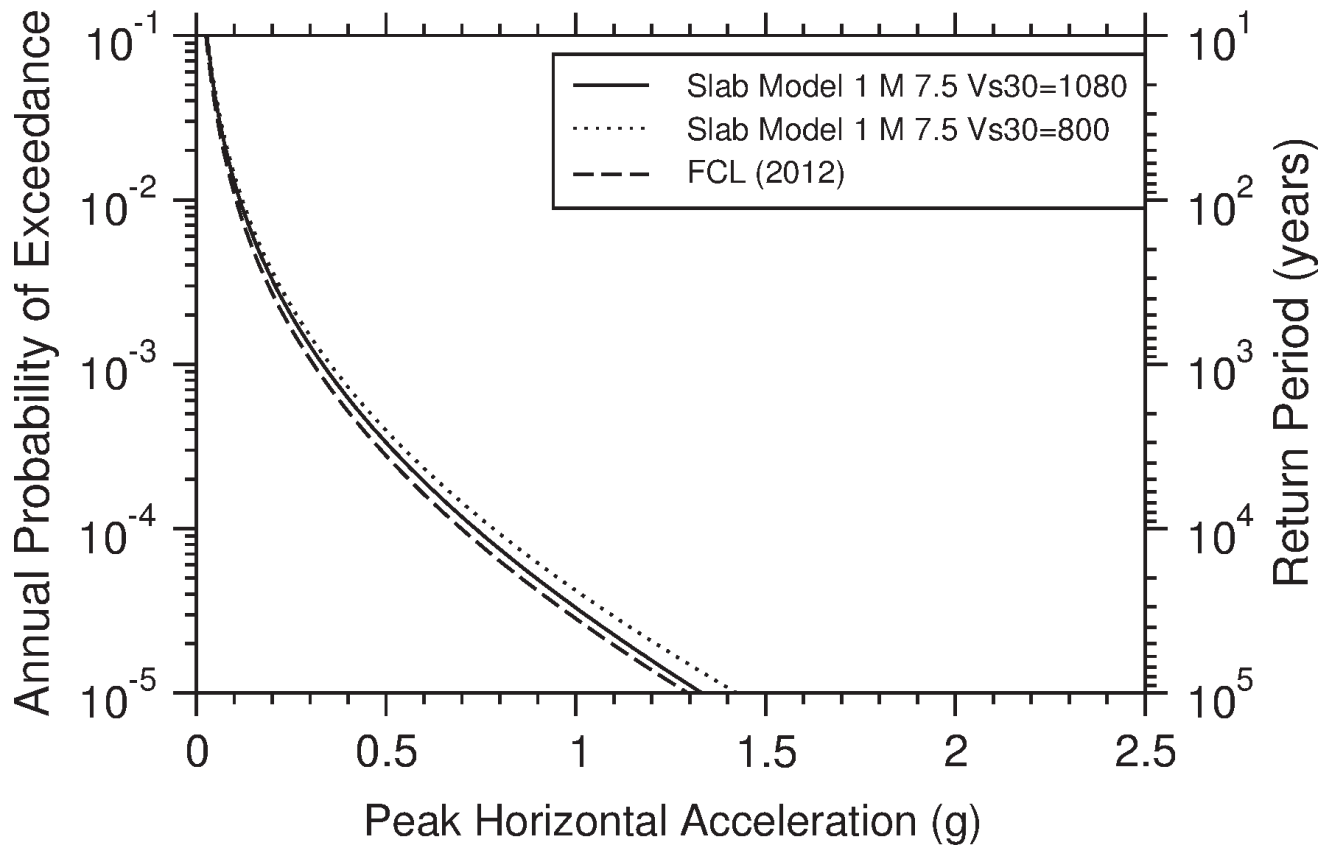
Correlation Distance Sensitivity



Correlation Distance Sensitivity



Vs30 800 vs 1080



Vs30 800 vs 1080

